Examining the impact of PUFAs and the role of autophagy in iron-induced ferroptotic cell death

Patricia de Menezes Reboucas

Thesis submitted to the Faculty of Graduate Studies in Partial Fulfillment of the Requirements for the Degree of Master of Science.

Graduate Program in Biology

York University

Toronto, Ontario

August 2022

Abstract

Ferroptosis, an iron-dependent non-apoptotic cell death involves lipid peroxidation and associates with cardiometabolic disease and cancer. I established a model of iron overload in L6 cells and measured cell viability, toxicity and lipid peroxidation. Importantly, in PUFA pre-treated cells, the susceptibility to iron-induced lipid peroxidation was enhanced. This resulted in ferroptosis as cell death was attenuated by ferrostatin-1, a ferroptosis inhibitor, yet no attenuation was seen when an inhibitor of apoptosis was used. Increased lipid peroxidation was also found in PUFA pre-treaded cells in wild type but not in autophagy deficient cells. Additionally, preliminary data indicated an apparent rescue of ferroptosis-induced cell death when using the adiponectin receptor agonist ALY688, an autophagy inducer. In conclusion, these findings supported the theory that PUFAs can alter the cell susceptibility to iron-induced ferroptotic cell death and raise the possibility that autophagy plays a protective role against ferroptosis.

Acknowledgements

I would like to take this opportunity to thank my supervisor, Dr. Gary Sweeney, for all the support and guidance during these two years of learning and growth. I also would like to thank my advisor Dr. Robert Tsushima for his advice and suggestions to help me achieve my goals.

I would also like to thank my examiner committee Dr. Michael Scheid and Dr. Olivier Birot, for their valued time to evaluate and discuss my thesis.

Special thanks to Dr. Cindy Sung, as my mentor in the lab, most of what I know today is because of you. Thank you, all current and past members of Sweeney's lab, SungJi Cho, Khang Nguyen, Carina Tang, Eddie Tam, Chloe Reno, Sabrina Champsi, Yubin Lei, and Trista Chung. Also, special thanks to Saher Ahmed and Dana Al Rijjal for taking the time to proofread my thesis. Your daily positive energy and friendship has made my graduate experience very memorable.

Lastly, thank you to my family and partner, Jamie Lavin, for all your love and endless support, without you I would not be here today.

Table of Contents

List of Figures

Chapter 1 Figures

Chapter 2 Figures

Chapter 3 Figures

Chapter 5 Figures

List of Abbreviations

AA	Arachidonic Acid
ACC	Acetyl-CoA Carboxylase
ACSL3	Acyl-CoA Synthetase Long Chain Family Member 3
ACSL4	Acyl-CoA Synthetase Long Chain Family Member 4
ACSLs	Acetyl-CoA Synthetase Long Chain
AdipoR1	Adiponectin Receptor 1
AdipoR2	Adiponectin Receptor 2
AdipoRon	Adiponectin Receptor Agonist
AdipoRs	Adiponectin Receptors
ALOX	Arachidonate Lipoxygenase
AMEM	Alpha Modification of Eagle's Medium
AMPK	AMP-activated Protein Kinase
ANOVA	Analysis of Variance
ATG	Autophagy Related genes
ATG5K130R	Autophagy Related 5 deficient mutant
ATG7KO	Autophagy Related 7 knockdown
BAK	BCL-2 Antagonist or Killer
BAT	Brown Adipose Tissue
BAX	BCL-2-Associated X Protein
BCA	Bicinchoninic Acid
BCL2	B Cell Lymphoma 2
BSA	Bovine Serum Albumin
CI	Caspase Inhibitor
COX	Cycloxygenase
DAPI	4’,6-Diamidino-2-Phenylyindole
DMSO	Dimethyl Sulfoxide
DMT1	Divalent Metal Transporter 1
DNA	Deoxyribonucleic Acid

DPBS	Dulbecco’s Phosphate-Buffered Saline
ECL	Enhanced Chemiluminescence
EDTA	Ethylenediamine Tetra acetic Acid
EV	Empty Vector
FA	Fatty Acids
FAC	Ferric Ammonium Citrate
fAd	Full Length Adiponectin
FBS	Fetal Bovine Serum
Fer-1	Ferrostatin-1
FIP200	FAK Family Kinase-interacting Protein
FPN-1	Ferroportin 1
gAd	Globular Adiponectin
GFP	Green Fluorescent Protein
GSH	Glutathione
GPX4	Glutathione Peroxidase 4
HDL-C	High-density Lipoprotein Cholesterol
HFD	High Fat Diet
HFE	Human Homeostatic Iron Regulator Protein
HMW	High Molecular Weight
HRP	Secondary Horseradish Peroxidase
IO	Iron Overload
L6	Rat Skeletal Muscle Myoblasts
LC3	Microtubule-Associated Protein Light Chain 3
LDH	Lactate dehydrogenase
LMW	Low Molecular Weight
LOHs	Lipid Alcohols
LOOHs	Lipid Hydroperoxides
LPCAT3	Lysophosphatidylcholine Acyltransferase 3
kDa	Kilodalton
KO	Knockdown
MDA	Malondialdehyde

MMW	Medium Molecular Weight
mTOR	Mammalian Target of Rapamycin
MTT	Methylthiazolyldiphenyl-Tetrazolium Bromide
MUFAs	Monounsaturated Fatty Acids
MVBs	Multi-vesicular Bodies
NCOA4	Nuclear Receptor Coactivator 4
NADPH	Nicotinamide Adenine Dinucleotide Phosphate
OA	Oleic Acid
PA	Palmitic Acid
PBS	Phosphate-Buffered Saline
PI3K	Class III Phosphatidylinositol 3-kinase
PE	Phosphatidylethanolamine
PUFAs	Polyunsaturated Fatty Acids
PUFA-PLs	Polyunsaturated Fatty Acid containing Phospholipids
PVDF	Polyvinylidene Fluoride
RCD	Regulated Cell Deaths
ROS	Reactive Oxygen Species
RSL3	RAS-Selective Lethal 3
SDS-PAGE	Sodium Dodecyl Sulfate Polyacrylamide Gel Electrophoresis
SEM	Standard Error of The Mean
SQSTM1/p62	Sequestosome-1, also known as p62
TBARS	Thiobarbituric Acid Reactive Substance
TCA	Trichloroacetic Acid
TEM	Transmission Electron Microscopy
TFR1	Transferrin Receptor 1
ULK1	Unc-51-like Autophagy activating Kinase 1
VPS15	Vacuolar Protein Sorting 15
VPS34	Vacuolar Protein Sorting 34
WAT	White Adipose Tissue
WHO	World Health Organization
WST	Water Soluble Tetrazolium Salt

WT	Wild Type

Chapter 1: Introduction and Research Aims

1.1 Metabolic syndrome and obesity

According to Metabolic Syndrome Canada, in order to be diagnosed with metabolic syndrome, a patient needs to have at least three of the following five indicators: high blood pressure, hyperglycemia, high triglycerides, low high-density lipoprotein cholesterol (HDL-C) or abdominal obesity [1]. Based off of this definition, in Canada alone, 20% of all adults are at risk of being diagnosed with metabolic syndrome and the risk continues to increase with age [1]. For example, according to Public Health Agency of Canada one in four Canadian adults is already obese, which is one of the criteria to develop metabolic syndrome, about 26.6% of the adult population [2].

Over the years, obesity has risen to become one of the top health issues in many countries, which is related to a increase in caloric intake and sedentary lifestyle [3]. The World Health Organization (WHO) has estimated that in 2016, more than 1.9 billion adults were overweight, and from them, over 650 million were obese [4].

These disturbing numbers are concerning as obesity is known to cause numerous disorders such as hypertension, glucose intolerance and dyslipidemia [5]. These symptoms are classified in the same metabolic syndrome group cited above, which implies that obesity leads to an increased risk of cardiovascular disease, type 2 diabetes, osteoarthritis, breast/endometrial cancer, and non-alcoholic fatty liver diseases [5, 6].

1.2 Obesity and skeletal muscle

Adipose tissue, a central component in metabolism, has been considered as the main energy storage system in the body [7]. It is divided into white adipose tissue (WAT) and brown adipose tissue (BAT). WAT is involved in energy storage, endocrine communication and insulin sensitivity, in addition, BAT is responsible for body temperature maintenance [8]. Adipocytes (adipose tissue cells) are regulated by many fatty acid proteins, which are responsible for binding and transporting lipids [9]. These mechanisms allow adipocytes to store large amounts of lipids; however, adipocytes have parameters that if crossed, can lead to metabolic diseases [9].

In conditions of obesity, adipocytes display signs of stress, such as compositional changes of lipids and other nutrients, hypoxia, mitochondrial dysfunction, production of reactive oxygen species (ROS), apoptotic signaling, increase of free fatty acids (FA), and altered adipokine signaling [10]. These signals result in lipid storage and processing capability limitations, causing metabolic dysfunction [10]. For these reasons, some studies have found that excess fatty acids of obese individuals lead to the deposition of lipids in ectopic tissues such as skeletal muscle, heart, and liver tissues [11, 12].

It is important to consider that biological effects of excessive lipid deposition in skeletal muscle could impact the accumulation of lipid intermediates, and these changes promote adverse outcomes such as lipotoxic stress [13]. In addition, some studies have also shown that excessive adipose tissue can lead to cell death and atrophy in skeletal muscle, which is involved in the development of various myopathies that are often

observed in obese patients [14]. However, it still unknown what other physiologic process are inhibited by this lipotoxic stress in skeletal muscle [15].

1.3 Iron metabolism and skeletal muscle

Iron is essential for numerous biochemical mechanisms of most cells in the human body. It participates in energy metabolism, deoxyribonucleic acid (DNA) synthesis, and oxygen transport [16, 17]. Therefore, its balance is very important to maintain a heathy organism and avoid a toxic environment, which is the consequence of excess iron [16]. This capability of iron to deal with these changes or not can damage proteins, DNA and lipids by the development of hydroxyl and lipid radicals [17, 18].

Iron overload is the accumulation of iron in the body and it can cause numerous diseases [19, 20]. The three main causes of iron overload are, first, genetic; second, iron overload can be found in patients that need to have constant blood transfusion; and third, levels of iron can elevate by excess dietary consumption [19]. The most susceptible organs to excess iron are the liver, heart and pancreas [19]. As an example, when iron is accumulated in the heart, it can lead to heart failure [19]. When it is in excess in the pancreas, it can cause insulin resistance and lead to diabetes [21].

Skeletal muscle tissue plays an important role in energy metabolism [22] and therefore, it has a crucial part in the regulation of metabolic syndrome responses [23]. In humans, skeletal muscle is about 40% of the total body weight and is vital in the storage of many proteins, regulation of body temperature, and participates in the energy metabolism [24]. Therefore, changes in iron homeostasis would affect skeletal muscles

tissues directly. For instance, in case of iron overload in skeletal muscle cells, muscle atrophy would occur [25].

Iron is controlled by specific proteins in the body, such as transferrin receptor 1 (TFR1) and divalent metal transporter 1 (DMT1), which are responsible for transporting iron into the cell, as well as iron is stored by ferritin, and it is exported by ferroportin 1 (FPN-1) [20]. Therefore, when there is an excess of iron, there will be an increase of ferritin-bounded iron [20]. However, if there is a lessening of iron intake, iron homeostasis is maintained by degradation of iron-bounded ferritin [20, 26]. There is no doubt that iron homeostasis is key for a healthy metabolism as detailed above, on the other hand, iron imbalance, such as iron overload, can result in reactions that may lead to cell damage or even cell death [27].

1.4 Ferroptosis

There are different regulated cell death (RCDs) modalities, including apoptosis, necrosis and autophagy [28-30] (Figure 1.1) where their processes have been studied and are well documented. For instance, the details of apoptosis, a programmed cell death by the activation of caspase pathways [28, 31] are well known in the field, tested in multiple cell types and different conditions [32, 33]. The morphological characteristics of apoptosis are chromatin condensation, plasma membrane blebbing and cell shrinkage [29, 34].

On the other hand, ferroptosis is a more recently discovered type of cell death. Ferroptosis is an iron-dependent form of non-apoptotic regulated cell death [35, 36],

which can cause oxidative stress and lipid peroxidation [37]. Lipid peroxidation can be defined as a process where oxidants, such as free radicals, react with lipids and causes extraction of a hydrogen from a carbon with oxygen [38]. This accumulation of lipid based reactive oxygen species (ROS) can be triggered by the interruption of glutathione (GSH) or the lipid repair enzyme glutathione peroxidase 4 (GPX4) [39, 40]. GPX4 is responsible for converting lipid hydroperoxides (LOOHs) into lipid alcohols (LOHs) using GSH as a co-factor [36, 41]. Therefore, GPX4 is key in the protection of cells against oxidative damage [42].

Ferroptosis was discovered when cells were treated with pharmacological compounds, erastin and RSL3, and a non-apoptotic death was observed [39]. In addition, recognised apoptosis enzymes such as caspases, BAX (BCL2 Associated X), and BAK (BCL2 Antagonist/Killer 1) were not activated [39, 40, 43]. Other experiments followed this discovery, and studies showed that “erastin-RSL3 cluster” causes a distinct form of cell death in the presence of iron overload, which they called “ferroptosis” [39]. Some unique morphological characteristics were also observed, such as reduction in mitochondria morphology, changes in its cristae [35, 43, 44] and cell membrane damage [45].

In addition to the discovery of ferroptosis inducers, there are studies showing that vitamin E, liproxstatin-1 and ferrostatins can inhibit ferroptosis. Among the ferrostatins, there is a synthetic small molecule called ferrostatin-1(Fer-1) [33, 46]. This “drug-like” compound has been tested in different cell types and can potently inhibit lipid peroxidation [33, 46]. Even though there is no clear mechanism on how ferrostatin-1 blocks lipid

peroxidation, some studies showed by unbiased metabolomics that ferrostatin-1 may act directly via the reduction of LOOHs to LOHs, preventing oxidative damage [46].

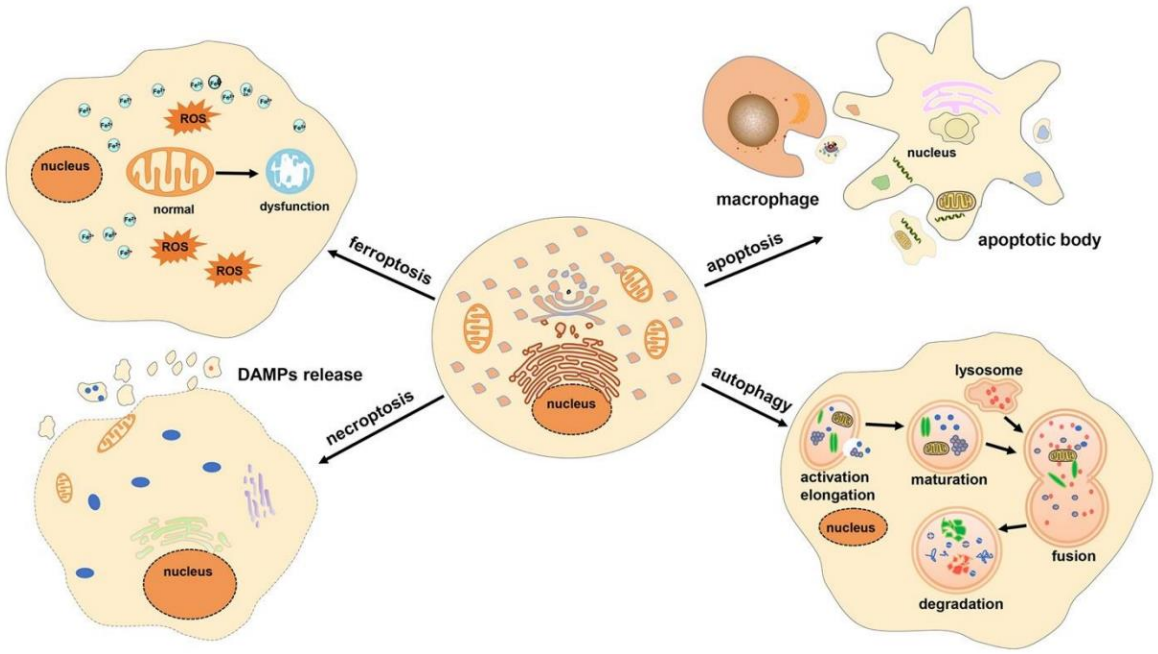

Figure 1.1: Programed cell deaths and its characteristics.

Each cell death type, apoptosis, necroptosis, autophagy and ferroptosis, has its own morphological characteristics which makes them unique. Apoptosis has chromatin condensation, cytoplasm shrinkage, plasma membrane blebbing. Necroptosis has organelles and cell swelling and loss of plasma membrane integrity. Autophagy has multiple autophagosomes and lysosomes. Ferroptosis has reduction in mitochondria morphology, changes in its cristae and cell membrane damage. *Retrieved from Ju, J. et al, 2020 [36].*

1.5 Ferroptosis mechanisms

Ferroptosis can be induced by different mechanisms, such as the inhibition of the system x_c^-, the glutamate/cystine antiporter; the direct inhibition of GPX4 by RSL3, and several others [39, 47, 48]. There are a few pathways related to ferroptosis found so far,

such as mevalonate pathway, which involves GPX4; the transsulfuration pathway, which is related to cysteine, and others involving glutamine and transferrin [39, 49].

However, one of the pathways that is directly related to the main ferroptosis hallmarks is the phospholipid peroxidation [50, 51]. It was found that acyl-CoA synthetase long-chain family member 4 (ACSL4) participates directly in the activation of ferroptosis by contributing to the production of key substances that lead to ferroptosis [52-54], such as free fatty acids [55]. ACSL4 followed by lysophosphatidylcholine acyltransferase 3 (LPCAT3) are part of the biosynthesis of polyunsaturated fatty acid containing phospholipids (PUFA-PLs) [56]. The increase of PUFA-PLs leads to an increase of lipid peroxidation and, consequently ferroptosis [56] (Figure 1.2).

As excess iron is another hallmark for ferroptosis, and pathways that regulate iron homeostasis are crucial for determining this iron-dependent cell death [57]. One of which is ferritin, the major iron storage protein, in which its degradation can lead to free labile iron in the cell resulting in an increase of Fenton reaction, and therefore, oxidative damage [57]. Another possible iron regulated process is related to prominin 2, a pentaspanin protein involved in lipid regulation [58]. Prominin 2 is responsible for increasing the development of ferritin-containing multi-vesicular bodies (MVBs) and exosomes which export iron outside of the cell, preventing ferroptosis [59].

The consequences of ferroptosis are clinically important as this non-apoptotic cell death is found in many diseases such as kidney injury, neurodegenerative diseases, ischemia/reperfusion-induced cardiomyopathy and cancer [39, 57, 60, 61]. Finding specific therapeutics and biomarkers related to ferroptosis will be of great advance for the future of clinical therapeutics [62].

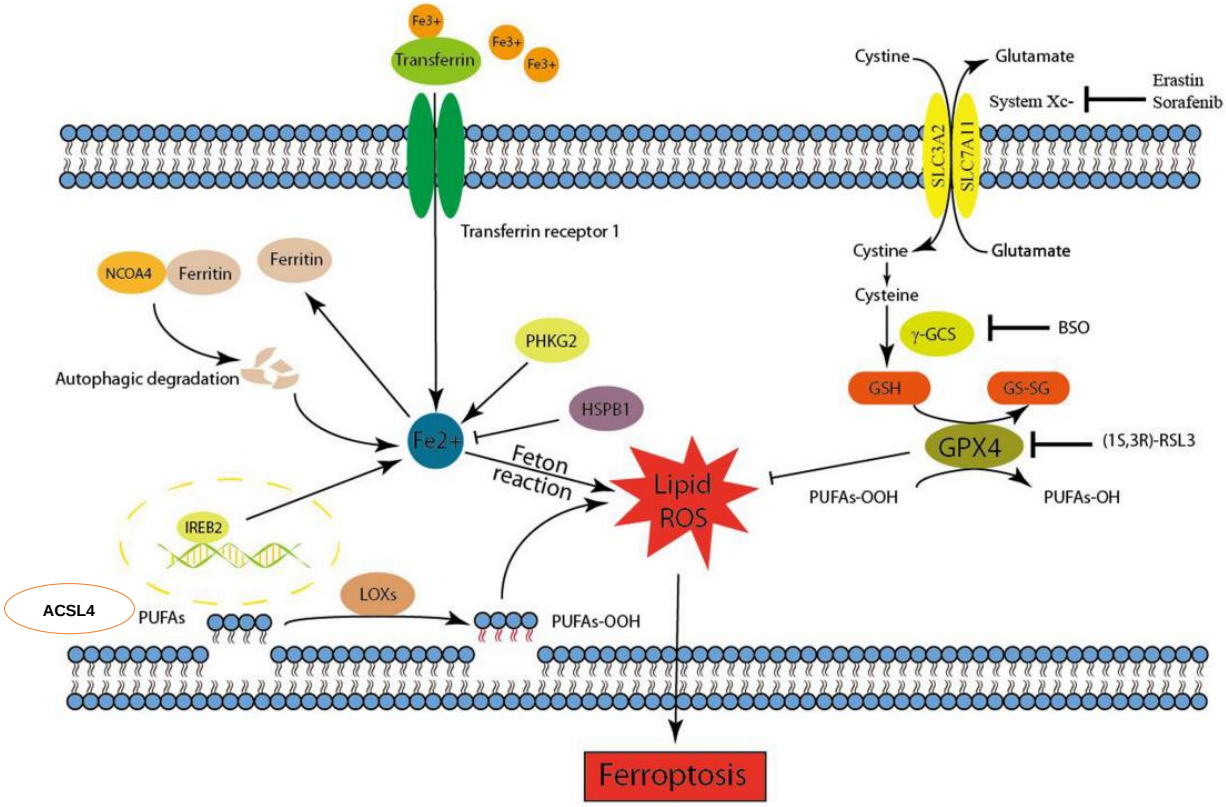

Figure 1.2: Ferroptosis mechanisms.

Ferroptosis can be inhibited by the glutamate/cystine antiporter or by GPX4 activity. On the contrary, ferroptosis is stimulated by free labile iron and peroxidation of PUFAs which leads to lipid ROS and consequently, ferroptotic cell death. *Image retrieved and adapted from Lu, B., et al (2018) [40].*

1.6 Importance of fatty acids

Fatty acids are one of the principal components for lipid synthesis in the body, and therefore, extremely important for energy metabolism [63]. They are often divided into two groups, unsaturated and saturated, conditional on having a carbon-carbon single or double bond with the carboxylic group [64]. Further, unsaturated fatty acids are

subdivided into polyunsaturated (PUFAs) and monounsaturated (MUFAs) based on the quantity of double bonds present [64]. Palmitic acid (PA), oleic acid (OA) and arachidonic acid (AA) are examples of fatty acids, and based on their quantity of double bonds they are classified as saturated, MUFAs, and PUFAs, respectively [64]. PUFAs are further classified as omega-3 and omega-6 depending on where the first double bond is located from the methyl end [65, 66]. Arachidonic acid (omega-6) derived lipids, for example, are found in the cell membrane and also in the lipids of immune cells [67]. Arachidonic acids are metabolized by cycloxygenase (COX) and arachidonate lipoxygenase (ALOX) enzymes to free lipids and are known to participate in many pathophysiological diseases, such as cardiovascular and metabolic diseases [68, 69].

It is also known that ferroptosis could be a result of lipid peroxidation of polyunsaturated fatty acids (PUFAs) [70, 71]. This excess PUFAs oxidation could lead to a change in the lipid membrane structure, leading to a more fragile membrane, where there is excess pore formation, and eventually a rupture could occur [72-74]. Interestingly, recent studies done in bone marrow derived cells compared lipid peroxidation in different cell deaths types, and their results showed that even though peroxidation of phospholipids is present in different RCDs, it is a lot higher in ferroptosis when compared to others RCDs and it also happens earlier in the process [73].

Lipid peroxidation can be activated by enzymatic or nonenzymatic pathways [41, 75]. In the enzymatic pathway, PUFAs peroxidation can be activated by long-chain acyl-CoA synthetases (ACSLs) enzymes [71]. Specifically, ACSL4 is involved in arachidonic acid induced ferroptosis, and ACSL3 participates in MUFAs pathway activation, the latter plays a protective role against PUFA-induced ferroptosis [71, 76]. The excess of PUFAs

containing phospholipids (PUFA-PLs) on the cell membranes increases lipid peroxidation, and therefore, ferroptosis [77].

In nonenzymatic pathways, the excess free irons in the cytoplasm react with ROS leading to PUFAs peroxidation, which can initiate the Fenton reaction and produce even more free radicals, further leading to ferroptosis-indued cell death [41]. However, the details of this mechanism and how it works, particularly in skeletal muscle cells, remains to be fully defined.

1.7 Ferroptosis and autophagy crosstalk

New studies showed that another important pathway to ferroptosis involves the regulation of macroautophagy (hereafter referred to as autophagy) and specifically the degradation of ferritin, known as ferritinophagy [78]. The link is so close that some researchers classified ferroptosis as an autophagic cell death [79]. Lysosomal degradation of ferritin leads to an increase of redox-active iron in the cell which could result in ferroptosis [78, 80]. However, the autophagy of non-iron-saturated ferritin could have the opposite effect, as degradation of ferritins without iron would lead to a deficit of iron storage proteins [81].

Autophagy is a regulated process that mainly serves as an adaptive role to protect the cell from unwanted components and thus protect against many pathologies, including infections, cancer and heart disease [82-84]. Autophagy depends on the formation and maturation of specific membrane structures, it starts with the formation of phagophores to engulf cellular components in the cytoplasm, then a double-membrane autophagosome

is formed, and it is followed by the fusion of the autophagosome with lysosomes, generating autolysosomes which are responsible for the cargo degradation [85].

There are about 40 autophagy-related (ATG) genes responsible for this whole process [85]. Autophagosome formation contains three major steps: induction, nucleation and maturation/fusion [5]. The induction step is controlled by the ULK1 (unc-51-like autophagy activating kinase 1) complex with FIP200 (FAK family kinase-interacting protein) plus the ATG13-ATG101 complex [5, 86]. The ULK1 interacts with serine/threonine kinase mammalian target of rapamycin (mTOR), which is the main autophagy inhibitor [5, 87]. However, under specific conditions, autophagy is activated by inhibition of mTOR that results in ULK1 activation and phosphorylation of ATG13 and FIP200; therefore, initiating autophagy [5, 87].

The nucleation step involves the lipid kinase of a complex containing vacuolar protein sorting 34 (VPS34), Beclin 1, and class III phosphatidylinositol 3-kinase (PI3K), this complex also includes VPS15 and ATG14L [5, 88]. This complex is usually inactivated by anti-apoptotic proteins from the BCL-2 family, but when autophagy is active it enables the nucleation of the isolation membrane [5].

The final autophagy step, maturation and fusion, requires the employment of two ubiquitin-like protein conjugation systems [5]. First, ATG12 binds to ATG5 mediated by ATG7 and ATG10, then ATG5 binds to ATG16L forming the ATG12-ATG5-ATG16L complex [5, 89]. Second, the microtubule-associated protein light chain 3 (LC3) is lipidated from its cytosolic form LC3-I to LC3-II, by the conjugation of phosphatidylethanolamine (PE) through the action of ATG7 and ATG3 [5, 89]. LC3-II is

localized in the inner membrane of the autophagosome, and it leads to the closure of the autophagic vacuole [5, 90].

LC3 is found on the inner membrane of the autophagosome and for this reason, it is the most used marker for autophagosome development as the increase in lipidated LC3 (LC3-II) will directly relate to the increase of autophagosome formation [91, 92].

Sequestosome-1/p62 is another important marker in the assessment of autophagy, as p62 is responsible for transporting ubiquitinated proteins to the autophagosome for degradation by binding to the polyubiquitin chains and LC3 [93]. Following the transportation of the cargo to the autophagosome, p62 is degraded along with it [91, 94]. In summary, autophagic flux is known for the increase of LC3-II levels and for the decrease of p62 levels. Under biological conditions, each ATG gene has its own function and they work as a perfect cascade accordingly to the cell's necessity to keep a healthy environment [95]. For instance, when there is a lack of essential nutrients autophagy is activated to maintain the cell's balance [96].

It is important to point out that iron overload has been described to regulate autophagy [21]. There are also studies that showed end products of ferroptosis leads to autophagosome formation [97]. Therefore, this connection between autophagy and ferroptosis should be further investigated.

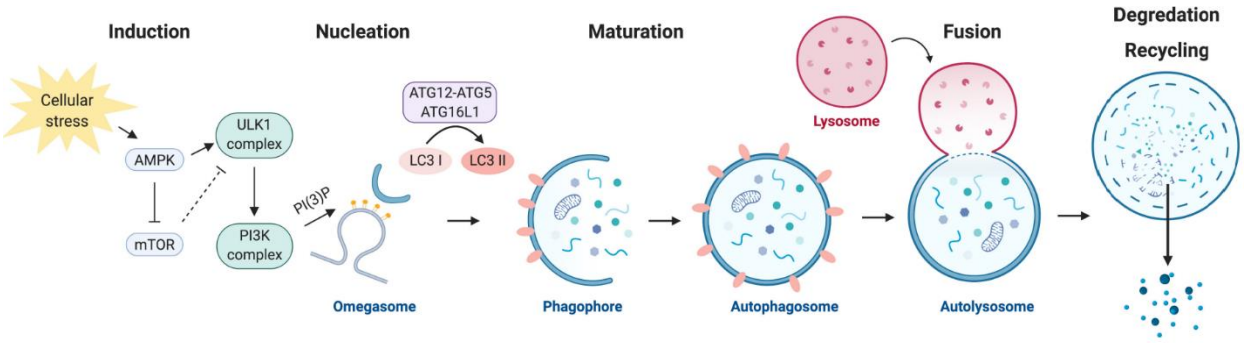

Figure 1.3: Autophagy pathway.

This diagram shows the main steps of the autophagy pathway, where upon cellular stress, such as starvation, AMPK inhibits mTOR and activates ULK1 complex leading to a cascade of reactions that depends particularly on the bound of ATG12-ATG5-ATG16L complex for the lipidation of LC3-I to LC3-II followed by the autophagosome formation, fusion of lysosome with autophagosome, which leads to autolysosome and degradation of the cargo of interest. *Image retrieved from Chang, N.C. (2020) [98]*.

1.8 Adiponectin

Adiponectin is a hormone secreted mainly by adipocytes and plays an important role in metabolic processes [99]. Human adiponectin consists of 244 amino acid residues, including a NH2-terminal hyper-variable region (amino acids from 1–18), plus a collagenous domain consisting of 22 Glycine-XY repeats, and a carboxyl (COOH)-terminal complement component (C1q)-like globular domain [100]. The monomers can form homotrimers also known as low molecular weight (LMW), hexamers or medium molecular weight (MMW) and oligomers or high molecular weight (HMW) [100]. The combination of these different oligomeric forms is called full length adiponectin (fAd); however, an additional form, globular adiponectin (gAd) containing only the carboxyl-terminal, may be generated by the enzymatic cleavage of adiponectin that exercises powerful metabolic effects [101].

Adiponectin is one of the most abundant adipokines present in the plasma [102]. In addition to adipocytes, other cell types, such as skeletal and cardiac myocytes cells, can also produce this adipokine [103]. Adiponectin is regulated by adiponectin receptors (AdipoRs), which occur as two isoforms (AdipoR1 and AdipoR2) [103].

There is evidence that adiponectin levels are reduced in obesity [104-106] and that AdipoRon, an activator of adiponectin receptors (AdipoRs) improves obesity-related imbalances in metabolism [105]. Previous studies from our lab showed the connection of adiponectin and autophagic flux in skeletal muscle cells [107]. They demonstrated that adiponectin induces autophagy, and also decreases oxidative stress [107]. However, the cross talk between autophagy and ferroptosis and their regulation by adiponectin are still uncertain.

To investigate in more depth the effects of adiponectin, ALY688, an adiponectin analogue has been used to mimic the effects of adiponectin [105]. ALY688 induced AMP-activated protein kinase (AMPK) and acetyl-CoA carboxylase (ACC) phosphorylation, enhanced glucose oxidation, and suppressed fat oxidation in adipocytes [105]. In another study, ALY688 treatment in high-fat high-sucrose-fed mice enhanced glucose handling, which means that ALY688 activated adiponectin signaling pathways in skeletal muscle, improving insulin sensitivity and metabolic effects [108]. Therefore, this peptide has shown that it can be used as an adiponectin analogue in-vitro and in-vivo models.

1.9 Hypothesis and aims

I hypothesized that iron overload can lead to cell death via inducing ferroptosis and that PUFAs can alter the cell susceptibility to iron-induced ferroptotic cell death. Specifically, pre-treatment with PUFA will allow iron to induce ferroptotic cell death at lower concentrations than in control cells. In addition, I proposed that the lack of autophagy exacerbates this effect.

To test my hypothesis, I established the following objectives:

Aim 1: Test if iron overload caused cell death via ferroptosis by measuring cell viability, cytotoxicity and lipid peroxidation levels.

Aim 2: Investigate if the use of PUFAs could alter the cell susceptibility in response to this ferroptotic cell death by comparing different fatty acids effect in cell death and lipid peroxidation levels.

Aim 3: Investigate if autophagy plays a protective or facilitatory role against ferroptotic cell death by assessing the effects of fatty acids and iron treatment in different autophagy deficient cells compared to control cells.

Chapter 2: Materials and Methods

2.1 Cell culture

Rat L6 myoblast (skeletal muscle cells), wild type (WT) L6 cells, ATG5K130R (ATG5K) L6, empty vector (EV) L6, and ATG7KO L6 were cultured in Alpha Modification of Eagle's Medium (AMEM, 5.5mM glucose, Wisent) containing 10% fetal bovine serum (FBS) and 1% Antibiotic-Antimycotic (Streptomycin, Amphotericin B, Penicillin, Wisent) at 37˚C, 95% humidity, and 5% CO_2.

The ATG5K130R dominant negative mutant already made and described by our lab [107], blocks conjugation to ATG12 on the lysine (K) residue, which was replaced by arginine (R) [107, 109]. This prevents the LC3-II incorporation into the early autophagosome and inhibits autophagy [23]. Empty vector (EV) L6 cells were used as the corresponding control for ATG5K130R cells.

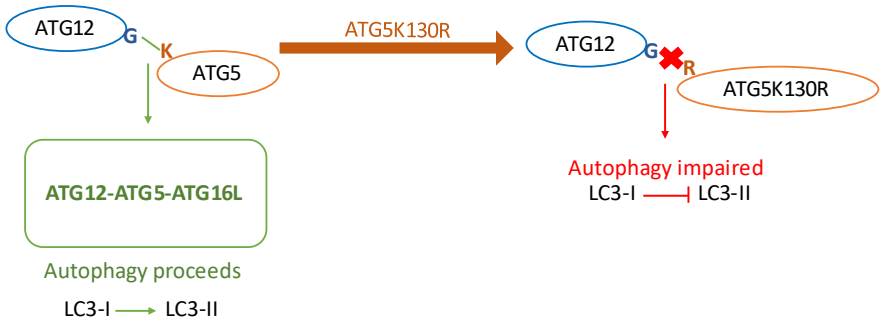

Figure 2.1: Diagram of ATG5K130R dominant negative mutant consequence in the autophagy pathway.

The conjugation of ATG12–ATG5-ATG16 depends on the covalently bind between ATG12 and the lysine (K) of ATG5, however, when ATG5 is biologically engineered to have K replaced by arginine (R) in the position 130, ATG12 do not bind to ATG5K, and as a consequence autophagy is inhibited [109].

2.2 Chemicals

The reagents used were the following: ammonium iron (III) sulfate dodecahydrate ($NH_4Fe(SO_2)_4$, #221260-25G, Sigma-Aldrich), ammonium iron (III) citrate (FAC, #F5879-100G, Sigma-Aldrich), iron (III) chloride hexahydrate ($FeCl_3$, #44944-50G, Sigma-Aldrich), iron (II) sulfate heptahydrate ($FeSO_4$, #215422-250G, Sigma-Aldrich), palmitic acid (#P9767-5G, Sigma), arachidonic acid (#10931-1G, Sigma-Aldrich), oleic acid (#O1008, Sigma-Aldrich), ferrostatin-1 (#SML0543-5G, Sigma-Aldrich), caspase Inhibitor I (Z-VAD-FMK, #627610, Sigma-Aldrich), erastin (#E7781, Sigma-Aldrich), ALY688 (compound was provided by Allysta Pharmaceuticals), hydrogen peroxide (H_2O_2, #H1009-100mL, Sigma).

2.3 Fatty acids preparation

Palmitic acid (PA) was diluted in 50% ethanol solution and added in a water bath at 57˚C for at least 15 minutes to dissolve it. Then it was added to the 2% FBS plus 2% bovine serum albumin (BSA) AMEM media for cell treatment. Arachidonic acid (AA) and oleic acid (OA) were also prepared in 50% ethanol solution, warmed in a heat block for one hour at 75˚C, then they were added to the 2% FBS plus 2% BSA AMEM media for cell treatment.

2.4 Cell viability assay

MTT (3-(4,5-dimethylthiazol-2-yl)-2,5-diphenyltetrazolium bromide, #M5655-1G, Sigma) assay was used to assess cellular viability. MTT is based on the reduction of the yellow compound (MTT) to a purple formazan crystal by metabolically active cells. The viable cells contain NAD(P)H-dependent oxidoreductase enzymes which reduces the MTT to formazan, measured by colorimetric assay at 550nm. I tested varying iron concentrations, at two different time points.

Iron stock solutions were prepared in distilled water and filtered before use. Iron treatments were then performed for 24 hours in 0.5% FBS AMEM media. The concentration of MTT used was 5mg/ml, and it was dissolved in Phosphate-Buffered Saline (PBS, Sigma-Aldrich) which was added to each well for four hours after the end of treatment. The media was removed and, in a 96-well plate, 200µL of dimethyl sulfoxide (DMSO) (#DMS 555.500, Biopshop) was added to each well and incubated at 37˚C for five minutes. Absorbance was measured at 550nm using Varioskan plate reader.

2.5 Lactate dehydrogenase (LDH) assay

LDH assay (#786-210, G-Biosciences) was used to determine cellular cytotoxicity of L6 cells with the various treatments indicated in each experiment. LDH is a stable enzyme, present in all cell types, which is rapidly released into the culture medium upon damage of the plasma membrane. LDH released from the cell oxidizes lactate to generate NADH, which then reacts with water soluble tetrazolium salt (WST) to generate a yellow

color. The intensity of the generated colour correlates directly with the number of lysed cells. The cells were treated as indicated, then 25µL of culture media was added to new 96-well plate and 25µL of reaction mix from LDH kit were added to it. The plate was incubated for 20 minutes at 37˚C, 5% CO_2 covered with aluminium foil. Then, the cells were measured by colorimetric assay at wavelengths 490nm and 680nm, followed by subtraction of 680nm from 490nm values then, normalized by control in order to reach the final cellular cytotoxicity measurement.

2.6 Western blotting

Wild type (WT) L6, empty vector (EV) L6, ATG5K130R (ATG5) L6 cells were grown to approximately 90% confluency in 6-well plates. Then, they were subjected to treatment as indicated in each experiment, and tested for expression of microtubule-associated protein light chain 3 (LC3-II, #2775S, Cell Signalling), sequestossomo-1 (SQSTM1/p62, #5114S, Cell Signalling), glutathione peroxidase 4 (GPX4, #AB125066, Abcam), acyl-CoA synthetase long chain family member 4 (ACSL4, #MA5-31543, Invitrogen), and ferritin heavy chain (Ferritin, #NBP1-31944, Novus Biologicals). The detection of LC3-II and p62 were used to show autophagy activity. GPX4, ACSL4 are ferroptosis markers, and Ferritin are indicators of ferritinophagy. The same cells were also pre-treated for 24 hours with PUFAs and then with different concentrations of iron. Also, when ALY688 was used for the treatment, the cells were pre-treated for 30 minutes prior to an iron treatment. After the treatment, the cells were washed three times with cold PBS, and lysed with 200µL of lysis buffer for five minutes at room temperature. Stock lysis components

consisted of 50mM Tris, 0.1% SDS, 30% glycerol, which were complemented with Pierce™ protease and phosphatase Inhibitor mini tablets (#A32959, Thermo Scientific) [consisting of Aprotinin, Bestatin, E-64, Leupeptin, Sodium fluoride, Sodium orthovanadate, Sodium pyrophosphate, β-glycerophosphate], 10% of β-mercaptoethanol, and bromothymol blue was added to the stock lysis buffer with the protease inhibitor cocktail. Lysates were scraped from wells, transferred to an Eppendorf tube and further lysed with 1 mL syringe for three times, then cells were centrifuged at 12000rpm for five minutes at 4˚C. Supernatants were then collected and boiled for five (5) minutes at 90˚C. Samples were cooled on ice and stored at -20˚C.

Samples were separated by sodium dodecyl sulfate polyacrylamide gel electrophoresis (SDS-PAGE), and maximum well loading volume was used per gel. Gels ran for about two hours at 90V then immunoblotted onto methanol activated polyvinylidene fluoride (PVDF) membranes (#162-0177, BioRad) for 1.5 hours at 120V. Membranes were blocked with 3% bovine serum albumin (BSA) (#ALB001.1, Bioshop) for one hour on a rocker at room temperature. Followed by overnight incubation with respective primary antibody 1:1000 dilution in 3% BSA at 4˚C on a rocker. The next day, membranes were washed three times with a wash buffer containing TWEEN 20 (#56-40-6, Bioshop) and Nonidet P40 (#NON505.500, Bioshop) detergents for ten minutes intervals at room temperature on a rocker. After, membranes were incubated in secondary horseradish peroxidase (HRP)-conjugated antibody 1:5000, anti-rabbit (#7074S, Cell Signalling) or anti-mouse, (#7076S, Cell Signalling) for one hour at room temperature, and then washed three times in ten minutes intervals. The membranes were incubated in enhanced chemiluminescence (ECL) reagent (# 1705061, Bio-Rad) for two

minutes, placed in a film cassette and exposed with film (#28906837, GE Health Care). They were then re-blotted with 1X Re-Blot buffer (#2504, EMD Millipore) on a rocker for ten minutes at room temperature. Membranes were washed one time, and re-blocked in 3% BSA for one hour when necessary. The band density was quantified using ImageJ Software, and normalized to appropriate loading control (glyceraldehyde-3-phosphate dehydrogenase, GAPDH, 14C10, #2118S, Cell Signalling or β-actin, #4967S, Cell Signalling).

2.7 Malondialdehyde (MDA) lipid peroxidation assay

Thiobarbituric acid reactive substance (TBARS) (TCA Method) Assay Kit (#700870, Cayman Chemical) was used to measure lipid peroxidation in L6 cells treated with different iron concentrations of iron or erastin, a positive control of ferroptosis-induced cell death, for 24 hours. After the treatment, the kit protocol was followed: 100µL of each lysate or standard to a screw cap tube, then 100µL of TCA Assay Reagent and 800µL of Color Reagent, incubated at 90˚C in a water bath for one hour, followed by an incubation of ten minutes on ice, and centrifuged for ten minutes at 1600g at 4˚C. Finally, 200µL of each sample/standard were added to a black bottom 96-well plate to read the fluorescence at an excitation of 530nm and emission of 560nm. The equation derived from preparation of the standard curve was used to calculate sample concentrations and thus lipid peroxidation level.

2.8 Image-iT® Lipid peroxidation assay

Image-iT® Lipid Peroxidation Kit (#C10445, Invitrogen) was used to measure lipid peroxidation in L6 cells treated with different fatty acids (palmitic acid, arachidonic acid, and oleic acid) plus or minus ALY688 for 24 hours, followed by 24 hours of iron treatment. The assay is based on the oxidation of lipids in cells, where the fluorescence shifts from red to green, which is read as a ratio. Therefore, more green fluorescence, means more lipid peroxidation. After treatment, cells were stained with Image-iT® lipid peroxidation sensor provided by commercial kit and 4′,6-diamidino-2-phenylindole (DAPI, #R10477, Invitrogen) for 30 minutes at 37˚C cover with aluminium foil. Cells were then washed three (3) times with Dulbecco's phosphate-buffered saline (DPBS), and fixed with 3% formalin for 20 minutes at room temperature. Three (3) final washes were performed with DPBS and measurements were done on Cell Insight CX7 High Content Screening Platform (CX-7).

2.9 Flow Cytometry analysis of lipid peroxidation

Lipid peroxidation assay kit (#ab243377, Abcam) was used to measure lipid peroxidation in WT L6 cells treated with arachidonic acid for 24 hours plus or minus 18 hours of 25µM $FeSO_4$ treatment, with an additional 30 minutes of pre-treated Ferrostatin-1 (Fer-1) before the iron treatment. Erastin was used as a positive control. The assay is based on peroxidation by ROS in cells, where the fluorescence shifts from red to green and can be read as a ratio. Therefore, more green fluorescence means more lipid

peroxidation. After the treatment, cells were stained with a lipid peroxidation sensor provided by a commercial kit plus live/dead probe (#L34966, Invitrogen) for 30 minutes at 37˚C covered with aluminium foil. Cells were then washed three times with DPBS, then 2mL of trypsin were added, incubated for three minutes at room temperature, centrifuged for five minutes at 2000rpm, and resuspended in 200µL of PBS. Fluorescence was measured by a flow cytometer through FITC/PE channels.

2.10 Statistical Analysis

Data was presented as mean ±SEM. The statistical significance between the treatment groups was calculated using unpaired Student *t* test when comparing two groups. One-Way ANOVA and Two-Way ANOVA was used for comparison of more than two groups with Tukey's post-hoc multiple comparison test. The p value < 0.05 was considered statistically significant and plotted with GraphPad Prism9.

Chapter 3: Results

3.1 Iron overload leads to a decrease of cellular metabolic activity and an increase of cellular cytoxicity

Previous research conducted in our lab used ferric ($FeCl_3$) and ferrous ($FeSO_4$) treatment to induce iron overload in cells. After receiving suggestions from reviewers of submitted manuscripts to test other sources of iron, I have also included ammonium iron (III) sulfate dodecahydrate [$NH_4Fe(SO_2)_4$] and ferric ammonium citrate (FAC). To first test the cell viability of wild type L6 skeletal muscle cells, different concentrations of these two iron forms [$NH_4Fe(SO_2)_4$ ((Fig. 3.1**A/B**) and FAC (Fig. 3.1**E/F**)], were used at the 4-hour and 24-hour time points. A significant increase was observed between FAC treatments and control for the period of 4-hour time period (Fig. 3.1**E**); however, there was no significant difference between any other iron concentrations or time versus control. H_2O_2 was used as positive control. Furthermore, the data showed that there was a tendency towards an increase in cell death with an increase of iron concentrations compared to control group, and particularly with an increase over time.

Additionally, lactate dehydrogenase (LDH) assay was performed to check for cellular cytotoxicity in wild type L6 skeletal muscle cells. Again, I tested different concentrations of the same two iron forms, $NH_4Fe(SO_2)_4$ (Fig. 3.1**C/D**) and FAC (Fig. 3.1**G/H**), at two time intervals of 4 hours and 24 hours. The data showed no significant difference between higher concentrations of the iron forms over either time period versus control. H_2O_2 was used as positive control.

In order to establish which form of iron has the strongest ability to induce iron overload in L6 skeletal muscle cells and cell viability and cytoxicity, I tested different iron forms: $FeCl_3$, $FeSO_4$, and FAC (Fig. 3.1**I**) and found that the response between these iron forms with the increase of ferritin expression, was very similar to one another. In addition, I compared the three types of iron with MTT and LDH assays (Fig. 3.1**J/K**) and, it confirmed that cell viability and cytotoxicity were also very comparable between the three different iron forms when compared to control.

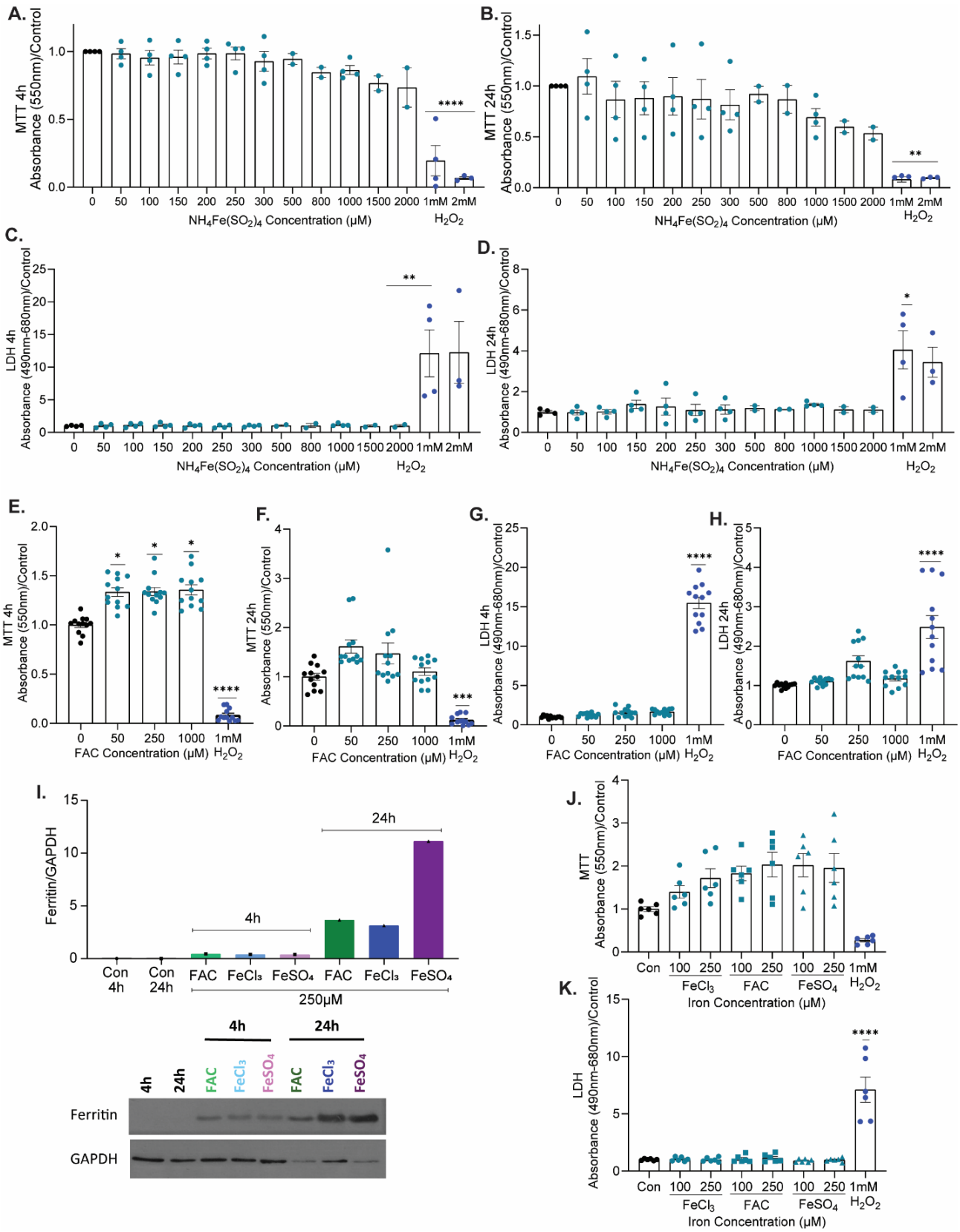
A.
MTT 4h
Absorbance (550nm)/Control
$NH_4Fe(SO_2)_4$ Concentration (μM)
H_2O_2
B.
MTT 24h
Absorbance (550nm)/Control
C.
LDH 4h
Absorbance (490nm-680nm)/Control
D.
LDH 24h
Absorbance (490nm-680nm)/Control
E.
MTT 4h
Absorbance (550nm)/Control
FAC Concentration (μM)
F.
MTT 24h
Absorbance (550nm)/Control
G.
LDH 4h
Absorbance (490nm-680nm)/Control
H.
LDH 24h
Absorbance (490nm-680nm)/Control
I.
Ferritin/GAPDH
Con 4h
Con 24h
FAC
$FeCl_3$
$FeSO_4$
250μM
Ferritin
GAPDH
J.
MTT
Absorbance (550nm)/Control
Iron Concentration (μM)
K.
LDH
Absorbance (490nm-680nm)/Control
Iron Concentration (μM)

Figure 3.1: IO leads to a decrease of cellular metabolic activity and an increase of cellular cytoxicity.

(A, B, C, D, E, F, G, H) Cell viability and toxicity of wild type L6 cells after treatment with different concentrations of $NH_4Fe(SO_2)_4$ or FAC or without (control), at two time points, 4h or 24h of incubation. H_2O_2 was used as a positive control. **(I)** Western blot and its quantification showing Ferritin and its reference protein, GAPDH. The blot shown is representative of one. **(J, K)** Cell viability and toxicity of wild type L6 cells after treatment with different concentrations of $FeCl_3$, FAC or $FeSO_4$ or without (control) for 24h. H_2O_2 was used as a positive control. **(A, B, C, D)** n=4 and **(E, F, G, H)** n=3, **(I)** n=1, **(J, K)** n=3. Data represents mean ± SEM; * indicates significant difference from control **p<0.05, ***p<0.001, ****p<0.0001*.

3.2 Iron overload induces lipid peroxidation

For the next stage of the study, I started with the validation of the lipid peroxidation assay using skeletal muscle L6 cells, and used a known stimulant of lipid peroxidation; erastin (Fig. 3.2**A**). My data indicated that there was a significant increase in lipid peroxidation with the increase of erastin concentration in L6 cells when compared to control (Fig. 3.2**A**). I then tested different concentrations of iron, using the same assay from Fig. 3.2**A** (lipid peroxidation assay), and there was a clear increase in lipid peroxidation with the increase of iron concentration when compared to no treatment (Fig. 3.2**B**). This result established that iron overload induced lipid peroxidation formation assessed by the accumulation of the final lipid peroxidation product, MDA.

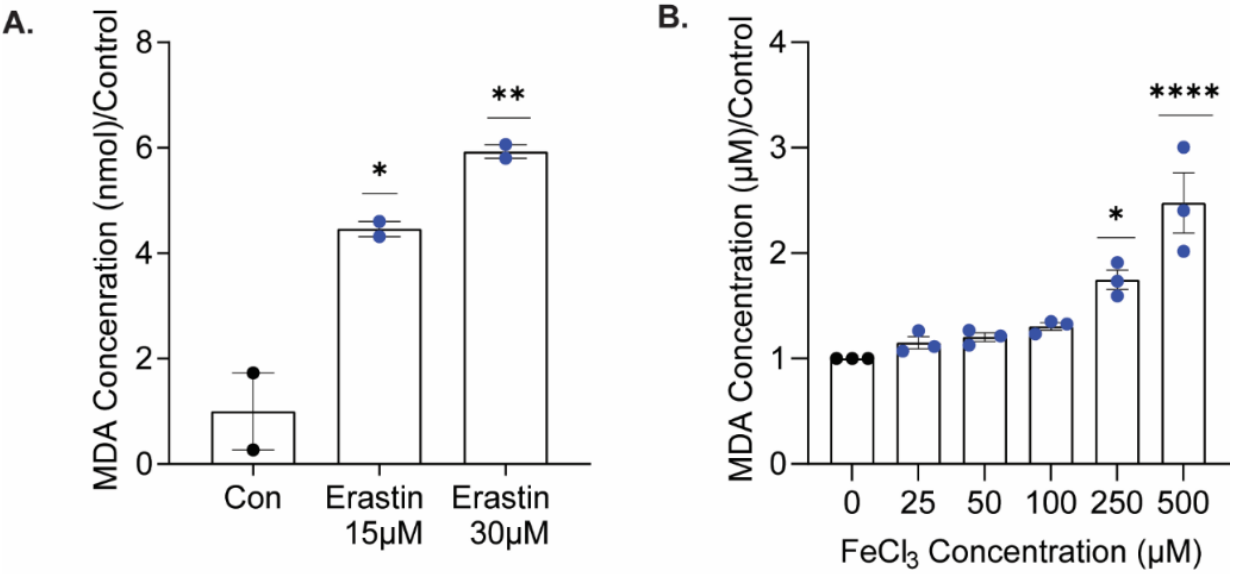

Figure 3.2: Iron Overload induces lipid peroxidation.

Wild type (WT) L6 cells were **(A)** treated with different concentration of erastin, also **(B)** treated with different concentrations of $FeCl_3$ or without (Con) for 24h. **(A)** n=2, **(B)** n=3. Data represents mean ± SEM. * indicates significant difference from control **p<0.05, **p<0.01, ****p<0.0001*.

3.3 Data validation using Cell Insight CX7 high content screening platform (CX-7)

Next, I used Cell Insight CX7 High Content Screening Platform (CX-7) in order to produce unbiased and high-quality data examining lipid peroxidation (Fig 3.3**A**). I used a 96-well plate for each experiment, selected the lipid peroxidation probe, which has red and green fluorescence that highlights healthy cells (red labeling) and lipid peroxidation (green labeling). The CX-7 platform identifies multiple cells in each well, reads the fluorescence and measures the intensity in an unbiased algorithm-driven manner. It also analyses multiple cells in each well giving the average for that well. Using this approach, it can be concluded that the increase of green fluorescence indicates the increase of lipid peroxidation; conversely, the ratio of red to green fluorescence is inversely correlated to lipid peroxidation formation.

The below figure (Fig. 3.3**B**) is an example extracted from the data of Fig. 3.4**B**, where palmitic acid was pre-treated for 24 hours followed by 24 hours of different concentrations of iron treatment. The results showed that two values were produced from the CX-7 platform, as a result of each treatment having duplicates in a 96-well plate. Each value used in the calculations is an average of the multiple cells from each well. The result indicates that even though the experiment is only n=1, the platform actually measured about 100 or more cells from each well giving an even more accurate analysis of each treatment. It can be seen from the images in Fig. 3.3**C** that the CX-7 platform identified multiple cells in one well and took image samples from each channel to validate accurate object measurement. For this algorithm, the CX-7 performed a cell segmentation for each

object of interest, and divided each one into nucleus and cytoplasm, identifying the part of the cell that is important for this study.

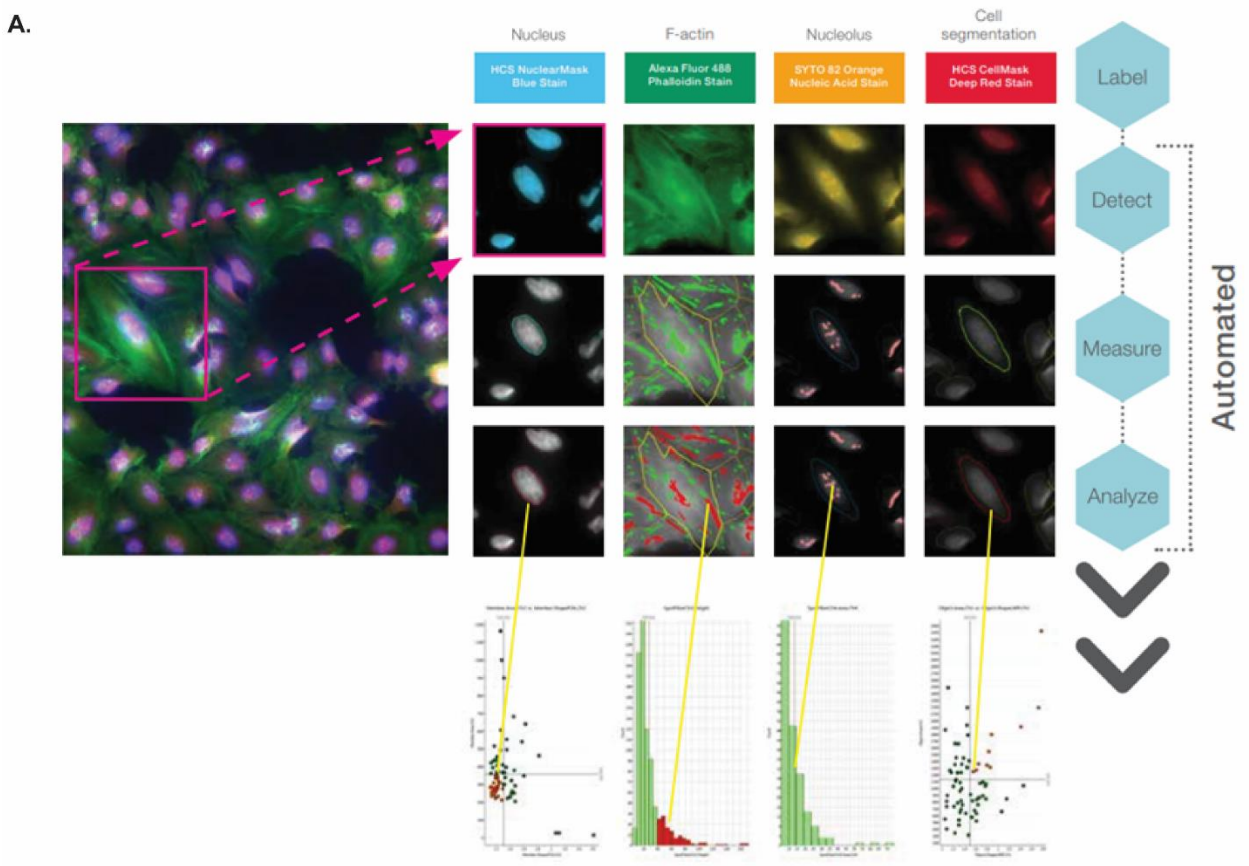

Automated imaging and quantification of multiple targets.

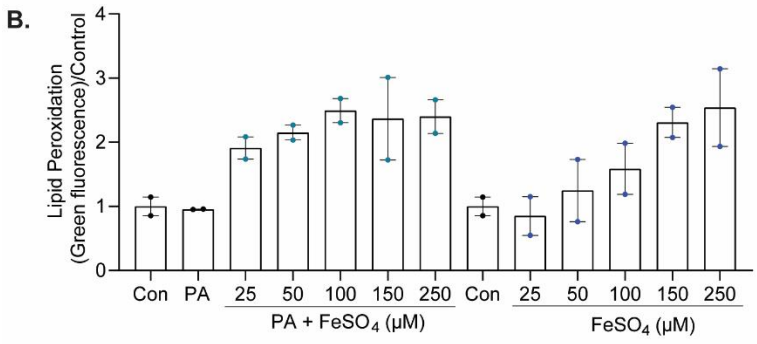

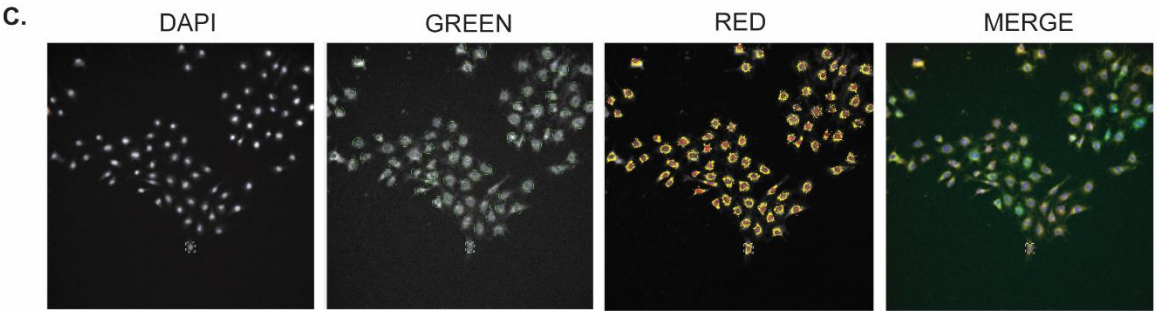

Figure 3.3: Cell Insight CX7 High Content Screening Platform (CX-7).

(A) Image retrieved from ThermoFisher website (https://assets.thermofisher.com/TFS-Assets/BID/brochures/cellinsight-cx5-cx7-led-cx7-lzr-high-content-screening-platforms-brochure.pdf). Copyrighted Property is owned by Life Technologies Corporation, a part of Thermo Fisher Scientific Inc. **(B)** Wild type (WT) L6 cells treated with 100µM Palmitic acid, followed by an additional 24h of 25µM $FeSO_4$ treatment (n=1). **(C)** Representative images of WT L6 cell segmentation by software identifying DAPI (nucleus), red and green (cytoplasm) fluorescence channels using the CX-7 platform algorithm, red fluorescence highlights heathy cells and green fluorescence, lipid peroxidation.

3.4 Fatty acid increases cell susceptibility for lipid peroxidation in wild type L6 cells when combined with iron treatment

After confirming that iron overload leads to lipid peroxidation, the next step was to understand how cells react to pre-treatment with fatty acids. I started with the use of palmitic acid, a saturated fatty acid, as it was found to induce ROS in previous studies [110]. So, I begun with 24 hours of palmitic acid treatment followed by 24 hours of different concentrations of two different forms of iron, $FeCl_3$ and $FeSO_4$ (Fig. 3.4**A/B**). The results presented showed no significant increase of lipid peroxidation when palmitic acid was pre-treated to cells prior to both forms of iron, particularly $FeSO_4$ when compared to control. However, there was a possible increase of lipid peroxidation in the lower doses of iron when compared to just iron treatment (Fig. 3.4**A/B**). As a result of this outcome, and in order to establish further correlation, I tested different palmitic acid concentrations, 50µM, 80µM and 100µM, with different concentrations of both irons (Fig. 2.4**C/D**). The findings from this assay suggested a possible increase of lipid peroxidation when the palmitic acid concentration was increased. There was also a visible detection of an increase in cell death together with an increase in lipid peroxidation showed in the images captured from the CX-7 microscopy (Fig. 3.4**E**). These outcomes could be an indication of ferroptosis-induced cell death.

Based on these results I decided to continue the study with ferrous iron form ($FeSO_4$), and with 80µM palmitic acid concentration.

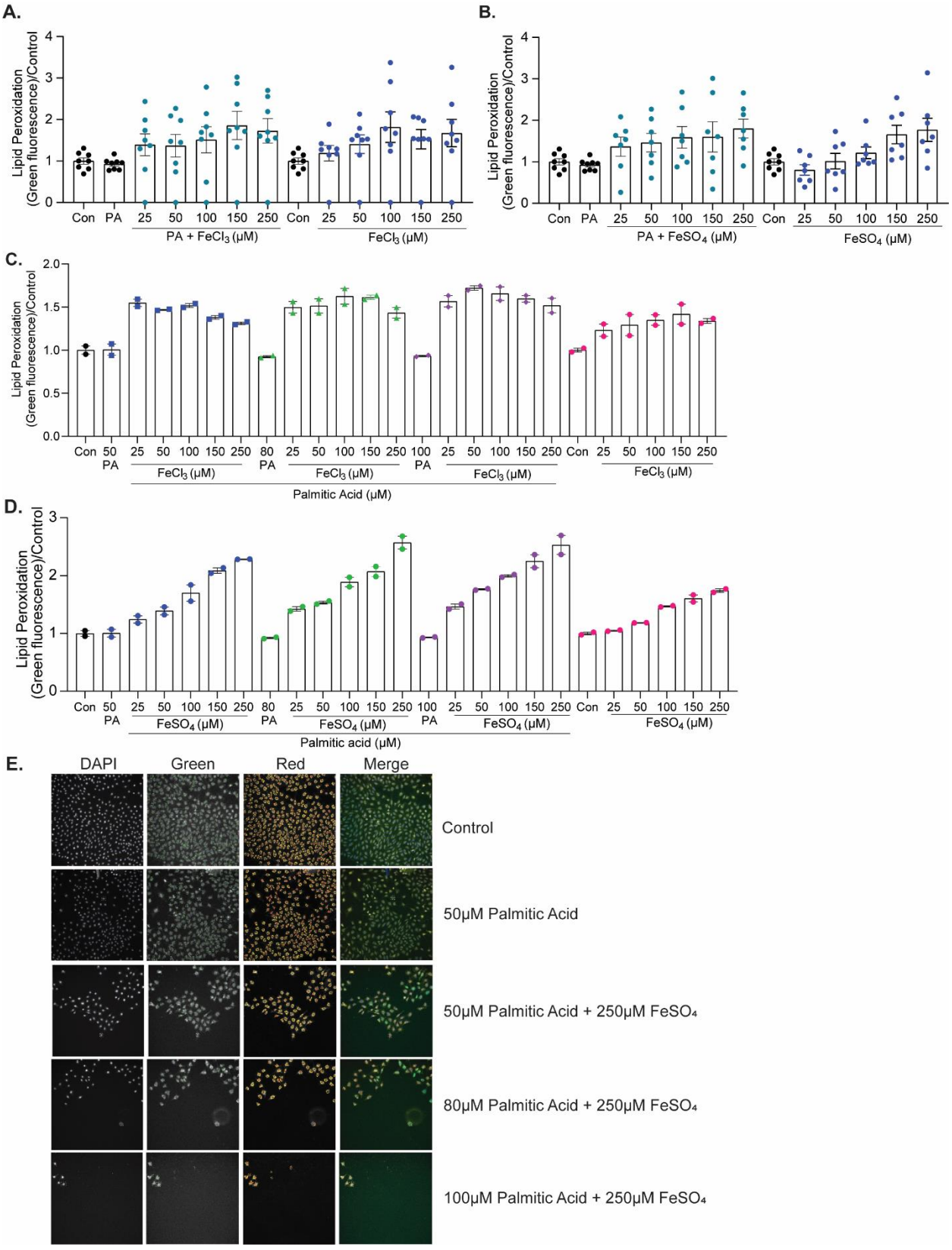
A.
Lipid Peroxidation (Green fluorescence)/Control
Con PA 25 50 100 150 250 Con 25 50 100 150 250
PA + FeCl3 (μM)
FeCl3 (μM)
B.
Lipid Peroxidation (Green fluorescence)/Control
Con PA 25 50 100 150 250 Con 25 50 100 150 250
PA + FeSO4 (μM)
FeSO4 (μM)
C.
Lipid Peroxidation (Green fluorescence)/Control
Con 50 PA 25 50 100 150 250 80 PA 25 50 100 150 250 100 PA 25 50 100 150 250 Con 25 50 100 150 250
FeCl3 (μM)
Palmitic Acid (μM)
D.
Lipid Peroxidation (Green fluorescence)/Control
Con 50 PA 25 50 100 150 250 80 PA 25 50 100 150 250 100 PA 25 50 100 150 250 Con 25 50 100 150 250
FeSO4 (μM)
Palmitic acid (μM)
E.
DAPI
Green
Red
Merge
Control
50μM Palmitic Acid
50μM Palmitic Acid + 250μM FeSO4
80μM Palmitic Acid + 250μM FeSO4
100μM Palmitic Acid + 250μM FeSO4

Figure 3.4: Fatty acids increase cell susceptibility for lipid peroxidation in wt L6 cells when combined with iron treatment.

(A, B) Wild type (WT) L6 cells treated with 100µM Palmitic acid, followed by an additional 24h iron ($FeCl_3$ and $FeSO_4$, respectively) treatment. **(C, D)** WT L6 treated with different palmitic acid concentrations: 50µM, 80µM or 100µM for 24h, followed by an additional 24h iron ($FeCl_3$ and $FeSO_4$, respectively) treatment. **(E)** Illustrative image of cell death increases after treatment with different concentrations of palmitic acid followed by $FeSO_4$ treatment from experiment D, DAPI highlights the nucleus, red fluorescence highlights healthy cells and green fluorescence, lipid peroxidation. **(A, B)** n=4, **(C, D)** n=1. Data represents mean ± SEM.

3.5 Examining dose-dependent effects of iron inducing ferroptosis in presence of fatty acids

After establishing the optimal form of iron ($FeSO_4$) and palmitic acid concentration (80µM) to be used, I tested how different fatty acids (Fig. 3.5), palmitic acid, arachidonic acid and oleic acid, would influence iron-induced ferroptosis. Just as a recap, palmitic acid, oleic acid and arachidonic acid are examples of saturated, monounsaturated and omega-6 polyunsaturated fatty acids, respectively [64].

The results did not show any significant difference when pre-treating palmitic acid or oleic acid; however, there was a significant increase of lipid peroxidation when arachidonic acid was pre-treated (Fig. 3.5**A**), combined with an apparent increase of cell toxicity when compared to control group (Fig. 3.5**B**).

To further clarify that this cell death was in fact ferroptosis-induced, I tested the same conditions above, but added ferrostatin-1, a lipid peroxidation inhibitor; and also, caspase inhibitor 1 (Z-VAD-FMK), a well-known pan-caspase inhibitor (Fig. 3.5**C/D**). The results showed an increase of cell cytotoxicity when arachidonic acid and iron were treated to cells, as expected; however, when ferrostatin-1 was added to the same condition (AA+Fer-1+iron) there was a clear inhibition of cell death when compared to AA+iron only group. Conversely, when the caspase inhibitor was pre-treated, there was no significant change in cellular cytotoxicity when compared to AA+iron. Therefore, these results showed that ferroptosis was the main pathway leading to cell death under these conditions.

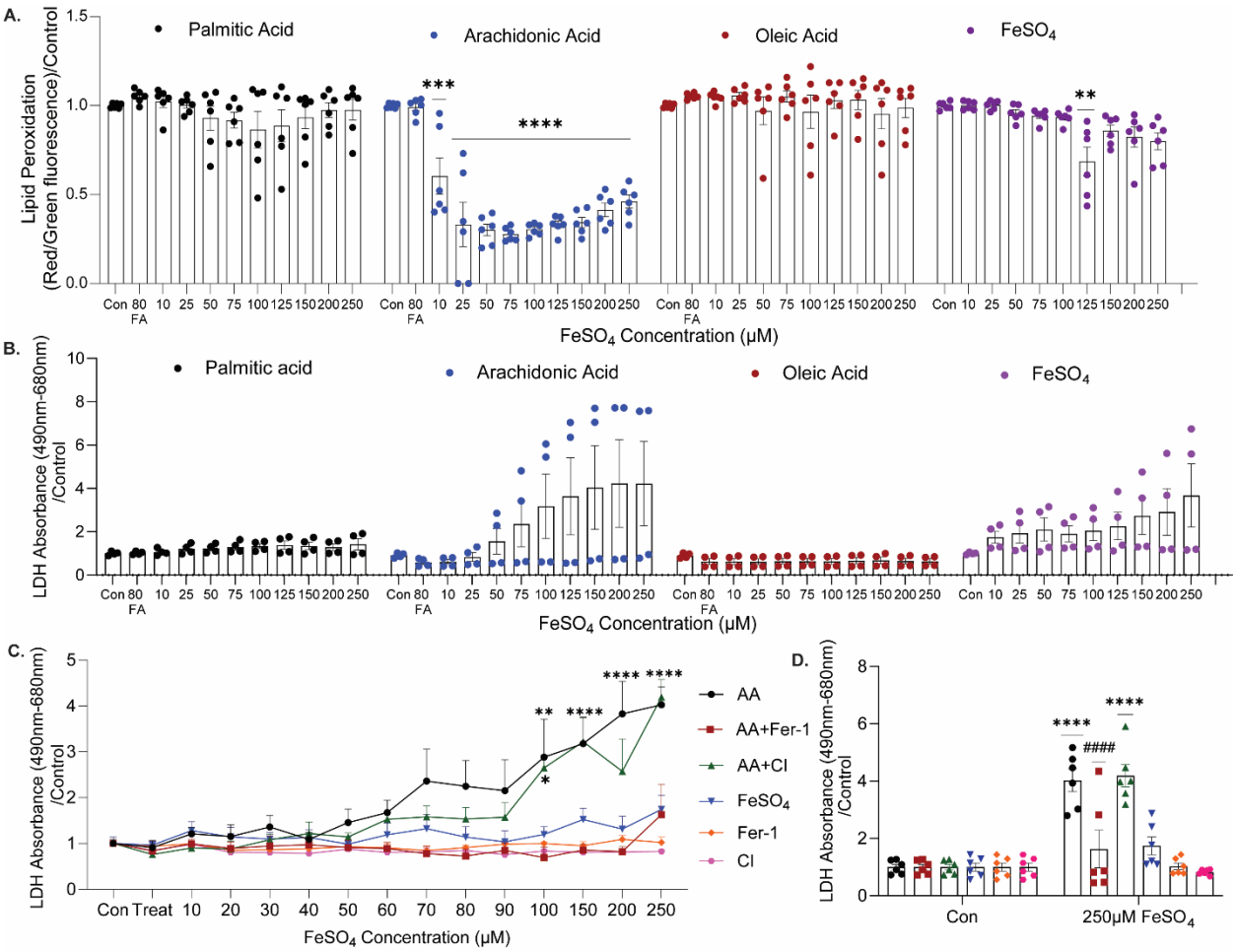

Figure 3.5: Establishing dose response in fatty acid plus iron inducing ferroptosis.

(A) Wild type (WT) L6 cells treated with 80μM fatty acid (FA), palmitic acid (PA), arachidonic acid (AA) or oleic acid (OA), followed by an additional 24h with different concentrations of $FeSO_4$ treatment. **(B)** LDH assay with same conditions as (A). **(C, D)** Cell cytoxicity assay of WT L6 cells treated with arachidonic acid for 24h followed by 24h $FeSO_4$ treatment; before iron treatment, cells were pre-treated for 30min with 1μM Ferrostatin-1 (Fer-1) or 50μM Caspase Inhibitor (CI) for 1 hour. **(A)** n=3, **(B)** n=2, **(C, D)** n=3. Data represents mean ± SEM. * indicates significant difference from control ***p<0.01, ***p<0.001, ****p<0.0001,* and # indicates significance difference from AA+Iron *#p<0.05, ##p<0.01*.

3.6 PUFAs plus iron induces ferroptosis-induced cell death

Next, I tested lipid peroxidation and cell death in wild type L6 cells by flow cytometry. The results showed a higher significant increase of lipid peroxidation (Fig. 3.6**A/B**) represented by the decrease of the red/green fluorescence ratio in AA plus iron compared to control. This assay also indicated a significant decrease of lipid peroxidation when ferrostatin-1 was pre-treated when compared AA+iron group with AA+Fer-1+iron group. There was also an increase of cell death (Fig. 3.6**C**) with the arachidonic acid pre-treatment followed by 25µM iron treatment compare to control, but also a similar increase of just AA, AA+Fer-1 and AA+Fer-1+iron treated cells. However, interestingly, there was a significant decrease of lipid peroxidation when Fer-1 was pre-treated, when we compare the AA+iron group with AA-Fer-1+iron. Combined these results confirmed that the cell death was induced by ferroptosis.

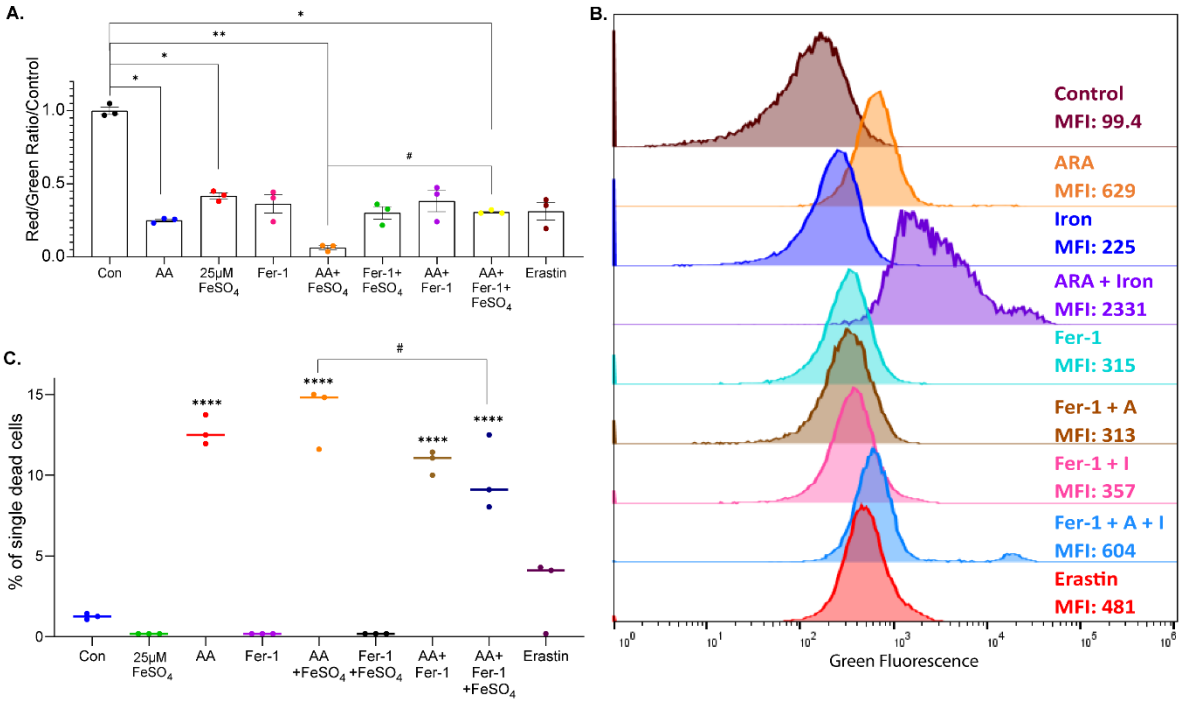

Figure 3.6: PUFAs plus iron induces ferroptosis-induced cell death.

(A) Wild type (WT) L6 cells treated with 80μM arachidonic acid (AA or ARA) followed by an additional 18h of 25μM $FeSO_4$ treatment +/- 1μM Ferrostatin-1 (Fer-1) 30min pre-treatment. Erastin was used as positive control. **(B)** Representative histograms of experiment (A) showing the direct lipid peroxidation formation. **(C)** Live and dead cell assay with same treatment as (A). **(A)** n=3, **(B)** n=1, **(C)** n=3. Data represents mean ± SEM. * indicates significant difference from control *$p<0.05$, **$p<0.01$, and $^{\#}$ indicates significance from specific conditions $^{\#}p<0.05$.

3.7 Validation of autophagy deficient cell lines

In order to investigate the relationship between ferroptosis and autophagy, it was important to validate the autophagy deficient cells generated by another lab member. Empty vector (EV) L6 cells were use as a control and ATG5K130R L6 cells as autophagy-deficient cells. First, I tested the response of autophagy to iron overload, and the data showed an increase of autophagosome formation over time (Fig. 3.7**A**) in EV L6 cells indicated by the increase of LC3-II accumulation, and a decrease of LC3-II expression in ATG5K130R L6 cells; however, there was no significant difference of p62 expression over time in neither type of cells (Fig. 3.7**B**). Otherwise, an apparent increase of p62 was seen, particularly in ATG5K130R L6 cells. This data suggests that iron overload leads to autophagosome formation in EV L6 cells but not in autophagy-deficient L6 cells.

I also tested the autophagy-deficient cell line created by knockdown of ATG7KO, and as expected there was no autophagosome accumulation in ATG7KO when compared to wild type L6 cells under the treatment of the known autophagy regulator, chloroquine (Fig. 3.7**C**). In addition, there was a clear increase of p62 content after the same treatment in ATG7KO indicating impaired autophagy flux in the autophagy deficient cell line.

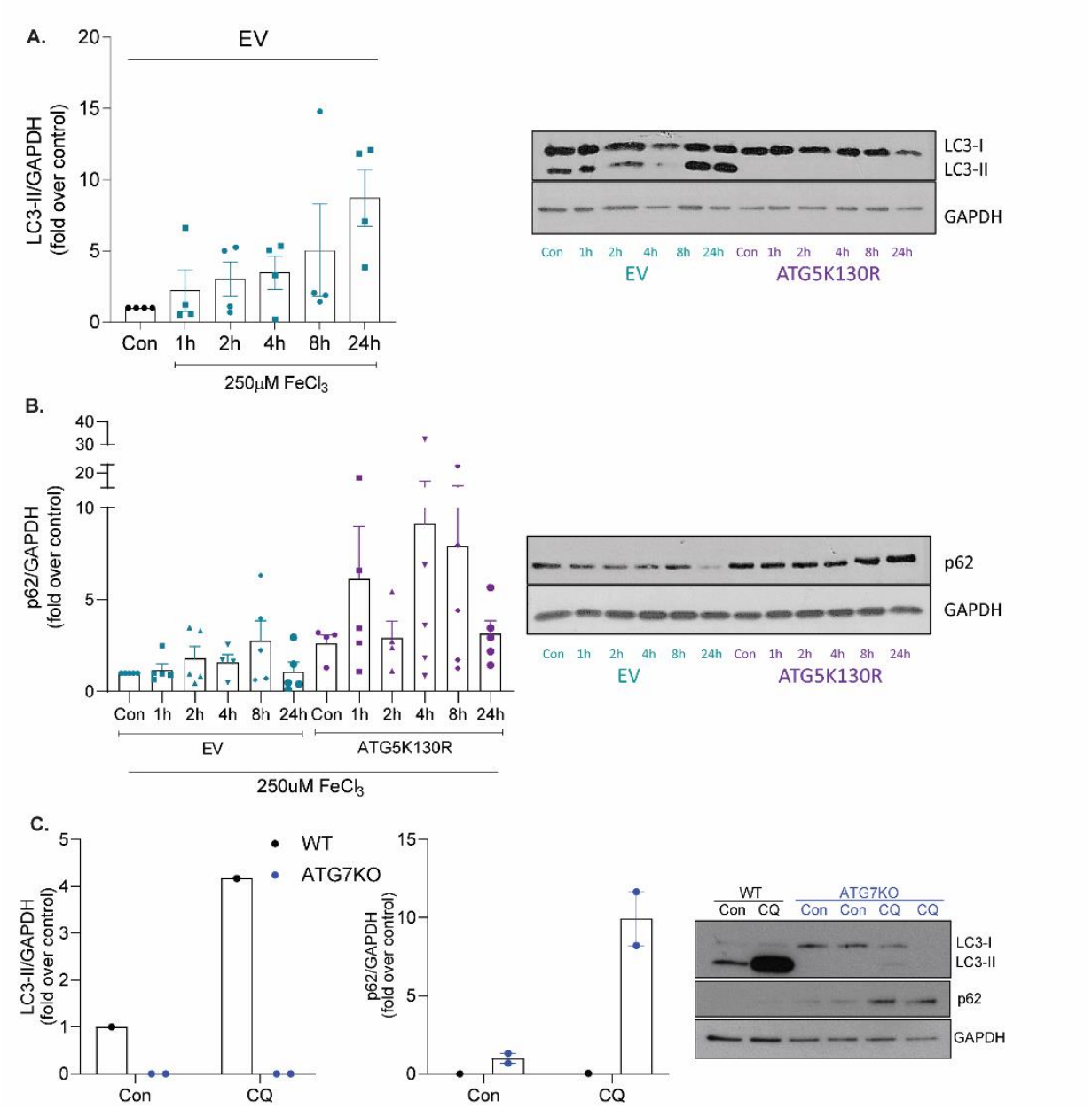

Figure 3.7: Validation of autophagy deficient cell lines.

Empty Vector (EV) L6 and ATG5130K L6 cells were treated with 250μM $FeCl_3$ over time. Western blot and its quantification showing **(A)** LC3-II and **(B)** p62, and their reference proteins, GAPDH. **(C)** WT and ATG7KO L6 cells were treated with 60μM chloroquine (CQ) for 24h, western blot and its quantification showing LC3-II and p62, and their reference protein, GAPDH. **(A)** n=4, **(B)** n=5, and **(C)** n=1. Data represents mean ± SEM.

3.8 Investigation of palmitate-induced alterations in autophagy

To investigate the connection between ferroptosis and autophagy, I started by conducting a pre-treatment of WT L6 cells with palmitic acid, followed by 24 hours of iron. There was an apparent increase of autophagosome formation when palmitic acid was present. On the other hand, there was no significance difference between fatty acids pre-treated cells and just iron overload treated cells (Fig. 3.8**A**). However, there was a suggestion of higher accumulation of p62 when fatty acids were added compared to just iron treated cells (Fig. 3.8**B**).

Ferritin expression also has an apparent increase in the presence of fatty acids, which could indicate that there is a higher pool of free iron available in the cell (Fig. 2.8**C**). Plus, there was a possible decrease of GPX4 (Fig. 3.8**D**), a known ferroptosis marker, when palmitate and iron were co-treated. The downregulation of GPX4 is a suggestion that lipid peroxidation is increased in the cell as it is as GPX4 directly reduce complex hydroperoxides [55]. These results could indicate that fatty acids exacerbate cell susceptibility for ferroptosis-induced cell death and autophagy may be involved.

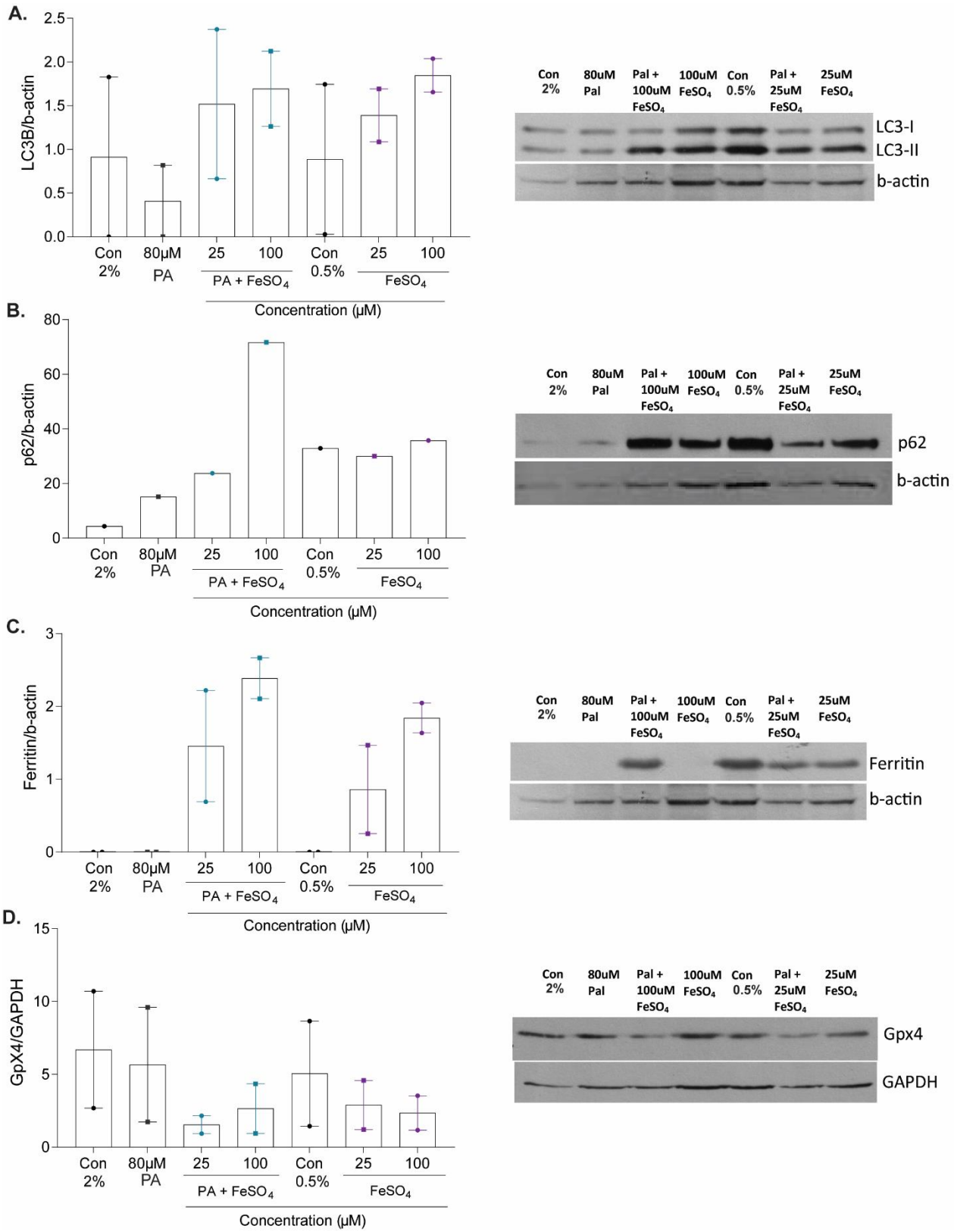
A.
LC3B/b-actin
2.5
2.0
1.5
1.0
0.5
0.0
Con 2%
80μM PA
25
100
PA + FeSO4
Con 0.5%
25
100
FeSO4
Concentration (μM)
Con 2%
80uM Pal
Pal + 100uM FeSO4
100uM FeSO4
Con 0.5%
Pal + 25uM FeSO4
25uM FeSO4
LC3-I
LC3-II
b-actin
B.
p62/b-actin
80
60
40
20
0
Con 2%
80μM PA
25
100
PA + FeSO4
Con 0.5%
25
100
FeSO4
Concentration (μM)
Con 2%
80uM Pal
Pal + 100uM FeSO4
100uM FeSO4
Con 0.5%
Pal + 25uM FeSO4
25uM FeSO4
p62
b-actin
C.
Ferritin/b-actin
3
2
1
0
Con 2%
80μM PA
25
100
PA + FeSO4
Con 0.5%
25
100
FeSO4
Concentration (μM)
Con 2%
80uM Pal
Pal + 100uM FeSO4
100uM FeSO4
Con 0.5%
Pal + 25uM FeSO4
25uM FeSO4
Ferritin
b-actin
D.
GpX4/GAPDH
15
10
5
0
Con 2%
80μM PA
25
100
PA + FeSO4
Con 0.5%
25
100
FeSO4
Concentration (μM)
Con 2%
80uM Pal
Pal + 100uM FeSO4
100uM FeSO4
Con 0.5%
Pal + 25uM FeSO4
25uM FeSO4
Gpx4
GAPDH

Figure 3.8: Investigating how palmitate +/- iron alters autophagy.

Wild type L6 samples after 24h 80µM palmitic acid followed by 24h $FeSO_4$ treatments. **(A)** LC3-II, **(B)** p62, **(C)** Ferritin and **(D)** GPX4 expression, and their reference proteins. The blot gel shown is representative of one experiment: **(A)** n=2, **(B)** n=1, **(C)** n=1, **(D)** n=2.

3.9 Autophagy has a protective role in ferroptosis-induced cell death in WT L6

After validating the autophagy deficient cells' function, and to confirm the data from Fig. 2.8, I compared EV and ATG5K130R cells (Fig. 3.9**A**) using the probe to examine lipid peroxidation. Even though palmitic acid pre-treatment had some change in cell susceptibility, when comparing the results from the Fig. 2.5, where arachidonic acid showed significance difference between control and lower dose of iron treatment, I decided to continue the study with arachidonic acid and $FeSO_4$.

The results showed a possible increase of lipid peroxidation with arachidonic acid pre-treatment plus iron when compared to control (Fig. 3.9**A**). Also, there was no difference in the autophagy deficient cells between arachidonic acid pre-treated cells, iron only treated cells and its control (Fig. 3.9**A**). In addition, there was a rescue of lipid peroxidation formation when adiponectin agonist ALY688 (autophagy inducer) was added prior to iron treatment in EV cells but no changes in ATG5K130R cells (Fig. 3.9**A**).

To complement these outcomes, I also tested wild type cells and ATG7KO cells using the same probe and conditions (Fig. 3.9**B**). The results were very similar to the ATG5K130R cells, where there was higher increase of lipid peroxidation when arachidonic acid was pre-treated compared to only iron treated cells, and no changes were seen in autophagy knockout cells. Also, when comparing the ATG5K130R results with the ATG7KO cells, there was an increase of lipid peroxidation when adding 100µM FeSO4 in ATG5K130R, but no increase was seen in ATG7KO, which could confirm that in knockout cells the autophagy function is completely lost while in ATG5K130R some cells could still have a small degree of residual autophagy function. Therefore, these

outcomes could indicate an autophagy protective effect stimulated by the adiponectin agonist ALY688.

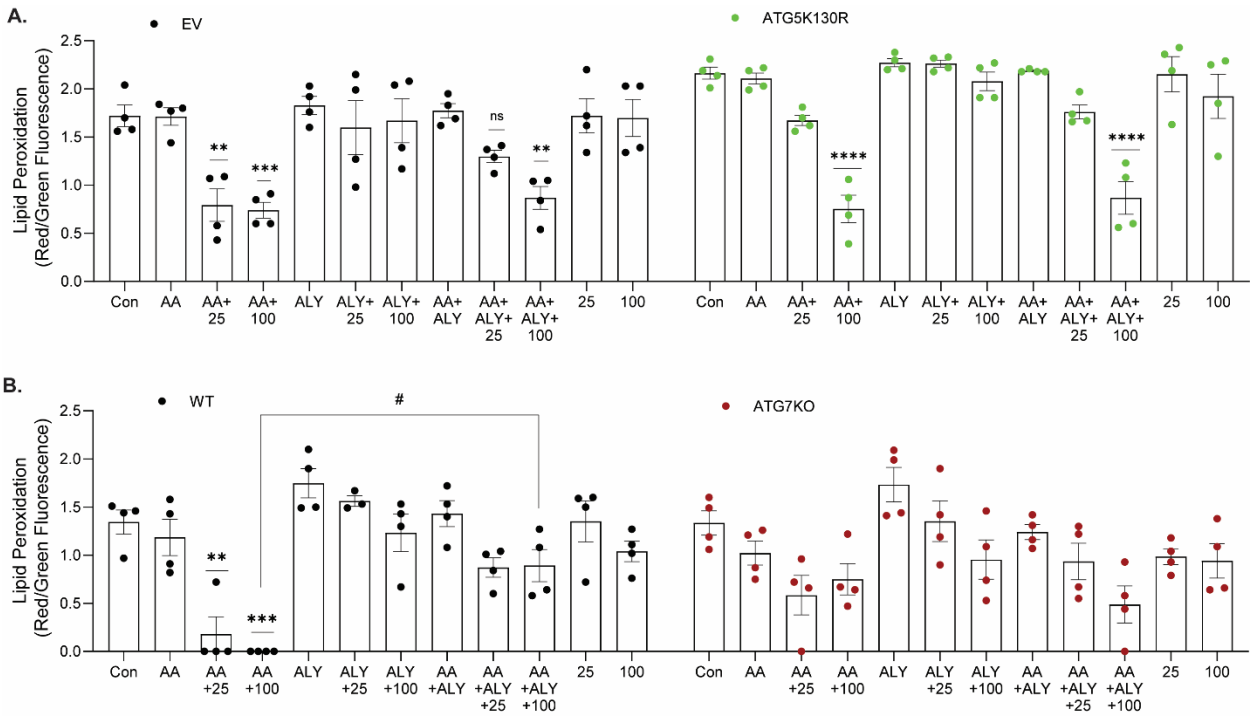

Figure 3.9: Autophagy has a protect role from ferroptosis-induced cell death in WT L6.

(A) Empty Vector (EV) or ATG5K130R L6 cells treated with 80µM arachidonic acid (AA) for 24h followed by an additional 24h of $FeSO_4$ treatment +/- 300nM ALY688 pre-treatment. **(B)** Wild type (WT) or ATG7KO L6 cells treated with same treatment as (A). **(A)** n=2 and **(B)** n=2. Data represents mean ± SEM. * indicates significant difference from control *$p<0.05$, **$p<0.01$, ***$p<0.001$, ****$p<0.0001$, and # indicates significance from specific conditions #$p<0.05$.

Chapter 4: Discussion

As referenced previously, iron homeostasis plays an important role in cellular function, contributing to energy metabolism, DNA synthesis, and oxygen transport [17]. It is also true that iron overload leads to an increase of cellular cytoxicity and diminishes cellular metabolic activity [17, 18]. In my research, I established a cellular model of iron overload and compared four different chemical forms of iron in order to establish which create the strongest biological effects in skeletal muscle cells. The results showed that there was a very similar response across different iron sources when treating skeletal muscle cells. Therefore, based on my research, it is safe to assume that any of the five irons used to continue this project should reproduce the expected outcome for skeletal muscle L6 cells in the specific treatment conditions outlined in this study.

One of the consequences of iron overload is the formation of free radicals and lipid peroxidation [18]. During the course of my research, it was confirmed that the increase of labile iron leads to the enhancement of MDA, which is one of the end products of lipid peroxidation [38]. The reactive and toxic aldehydes MDA and 4-hydroxynonenal (4-HNE) are known as secondary products of lipid peroxidation that can lead to inactivation of proteins and cell damage [70, 72, 111], such as in human lung cancer cells [112], vascular smooth muscle cell [113] and hepatic stellate cells [114]. Therefore, the results found in this study for skeletal muscle cells confirmed the same outcomes found in other literature using different cell types.

There are a few known pathways which promote ferroptosis susceptibility, one of which is through lipid synthesis, where PUFAs are oxidized and produced toxic lipid

hydroperoxides, which resulted in free radicals that combined with free iron and caused lipid peroxidation, and ultimately, ferroptosis in lung cells [115]. After investigating similar conditions, I also confirmed these findings in skeletal muscle cells.

According to previous studies, lipid peroxidation can change the bilayer membrane composition by altering, for example, the membrane permeability and fluidity, plus ion gradients levels [111, 116]. It has been shown that an increased level of PUFAs (arachidonic acid), but not saturated fatty acids (palmitic acid) or MUFAs (oleic acid), leads to an increase of lipid peroxidation and ferroptotic cell death [38, 117]. For example, activation of MUFAs pathway leads to a protective role against lipid peroxidation [71, 76]. On the other hand, the presence of excess of PUFA-PLs on the cell membranes increases ferroptosis [77]. However, the precise mechanism of how lipid peroxidation leads to ferroptosis is still unclear [115].

During my research, I was able to show that pre-treatment with PUFA, such as arachidonic acid, enhanced the sensitivity of skeletal muscle cells to iron-induced lipid peroxidation and consequently, ferroptosis-mediated cell death. In addition, by establish the right dose-response of the three different types of fatty acids tested in my study gave a clear response, and as expected, the excess of PUFAs showed a higher cell susceptibility for ferroptosis-induced cell death when compared to saturated fatty acid or MUFAs in skeletal muscle cells. However, further study needs to be undertaken to understand what specific mechanism is causing ferroptosis.

As mentioned previously, iron overload alters autophagy flux by increasing dysfunctional autolysosomes and loss of lysosomes [21]. Therefore, after confirming that PUFAs-treated skeletal muscle cells exhibit an increase of iron-induced ferroptotic cell

death, the next step was to investigate the relationship between ferroptosis and autophagy in this context. Based on previous studies' results, autophagy can intensify ferroptotic cell death by degradation of iron-saturated ferritin with release of labile iron [81] or conversely degradation of non-iron-saturated ferritin would lower the anti-oxidative capacity [81, 118]. It has also been stated that GPX4 knockout mouse leads to ferroptosis cell death as GPX4 is critical in the PLOOH-neutralizing enzyme, which transforms PLOOH into PLOH (alcohols) and inhibits lipid peroxidation [50]. Others studies also found that the treatment of fatty acids can influence autophagy response, it still unclear if fatty acids inhibit or induce autophagy, but it definitely alters it [119]. From the preliminary results found in my study there is a possible increase of cell susceptibility to ferroptosis when palmitic acid is treated with iron; however, more ferroptosis and autophagy markers plus more replicates need to be investigated to have a definite conclusion.

Finally I examined the effect of ALY688, a peptide-based adiponectin receptor agonist [108] which is known to act as an autophagy inducer [107]. It could be seen that there was a possible ALY688-mediated attenuation of lipid peroxidation formation, suggesting that autophagy may play a protective role against iron-induced ferroptotic cell death. This finding would go against most of the literature found regarding ferroptosis and autophagy, where studies show that autophagy degradation of key components such as ferritin, NCOA4, TFR1, GPX4, mitophagy, lipophagy, and others could lead to an increase of lipid peroxidation and iron overload [120]. However, others studies found that the increase of autophagy could protect cells from oxidative stress, by degradation of non-bound ferritin [81], which could be a defense mechanism against ferroptosis. Adiponectin is also known to have anti-oxidant property which could directly reduce lipid peroxidation

[121]. In addition, adiponectin participates in the lipid synthesis by regulating the expression enzymes involved in this process [121]. Therefore, with the results found in my study, further investigation into the autophagy and ferroptosis relationship, is necessary.

In summary, my research showed that iron overload leads to ferroptosis-induced cell death, but more specifically, the results showed that pre-treatment of polyunsaturated fatty acids, such as omega-6 arachidonic acid, increased cell susceptibility in low iron-induced ferroptosis cell death. It also indicates that autophagy participates in ferroptosis, furthermore it suggested that autophagy may play a protective role against ferroptosis. However, the exact mechanism of how these effects take place still uncertain, and further investigation needs to be done.

Chapter 5: Final Remarks and Future Plans

The research conducted throughout my project allowed for a better understanding of how iron overload leads to cell death via inducing ferroptosis. Additionally, it also indicated that autophagy may play a protective role in the process, creating a better understanding of the ferroptosis mechanism. Further, the study of the effect of PUFAs on cell susceptibility to ferroptotic cell death allowed for a stronger comprehension of the impact of obesity in these iron-dependent diseases. This can potentially translate to helping in the treatment of many iron-dependent complications, including cardiovascular diseases, diabetes, liver diseases and cancer.

To further investigate these findings, increased biological replicates for the in-vitro study by western blot with pre-treated fatty acids, particularly arachidonic acid, needs to be performed. Also, addition of ferroptosis and ferritinophagy markers should be analyzed, such as ACSL4, NCOA4, and transferrin receptor 1 in order to establish a stronger correlation between ferroptosis and skeletal muscle cells, as it has been found in other cell types. For instance, the expression of ACSL4 was upregulated in ferroptosis-sensitive cells such as human leukemia (HL60) and liver (HepG2) cells [122]. Another study also showed that ACSL4 knockdown inhibited lipid peroxides production and ferroptosis in cells [123]. As well, the direct inhibition of NCOA4, the main regulator of ferritinophagy, blocked the degradation of ferritin and therefore, inhibited ferroptosis in an ischemic stroke rat model [124]. Transferrin receptor 1 was also found as one of the effective markers for ferroptotic cell death by a study with multiple cell culture and tissue

[54]. Therefore, all of these three markers could be used to help clarifying the results found so far in skeletal muscle cells.

To go even further, human skeletal muscle cells could be added to the in-vitro studies with the same conditions presented in my study to compare the results found in rat cells to human cells. Then, the continued research should be translated to an in-vivo study, where high fat diet (HFD) can be fed to mice to mimic fatty acid's effect or oral omega-6 can be used to mimic arachidonic acid's effect, followed by iron treatment for 24 hours. The muscle tissue can be harvest and analyzed with same assays from this research, such as MDA assay and Western blot analysis.

To add to the investigation of the autophagy and ferroptosis relationship, tandem fluorescent-tagged LC3 (tfLC3-GFP-mCherry) L6 cells could be used as an additional autophagy flux assay. This assay is based on fluorescent signals of the tfLC3, such as GFP (green fluorescence) and mCherry (red fluorescence), which differs in pH stability of each fluorescent protein. For instance, mCherry keeps its fluorescence in acidic environments; whereas, the GFP does not [125, 126]. Keeping that in mind, it is known that the inside of a lysosome has a more acidic environment, which means that when autolysosomes are formed, green fluorescence loses it signal, and only red fluorescence is seen under a microscope [125, 126]. However, if red and green still have strong signals, the fluorescence is merged and a yellow puncta is seen under a microscope, which means only autophagosomes is seen [125, 126]. Therefore, autophagic flux can be measured by the increase of red puncta in cells while autophagic flux is blocked when only yellow puncta are increased [125, 126]. This is a reliable assay because there is no staining necessary, the cells are ready to produce the results based solely on the

treatment of interest. Therefore, established activators of autophagy could be added to compare the treatment of interest with the autophagy inducer, such as rapamycin [127]. In addition, autophagy deficient cells could be transfected with the tfLC3-GFP-mCherry, and comparison of the results between wild type and autophagy deficient cells would help understand the autophagy relationship with ferroptosis-induced cell death.

To compare the relationship between autophagy and ferroptosis, ATG7KO mice could be used in comparison with wild type. In addition, as it was found in this research, autophagy plays a protective role against ferroptosis, compound ALY688 could be injected in another group of mice, having a total of six groups: WT (normal diet plus iron, normal diet plus iron and ALY688; HFD plus iron, HFD plus iron and ALY688), and the same with ATG7KO. There are many ways to further enrich the scope of this research where it can help confirm the answers found with the in-vitro work.

The in-vivo experiment also allows for there to be an added transmission electron microscopy (TEM) analysis as it is a great tool for studying autophagy, in which the images would provide a more powerful visualization of autophagosomes [57]. Mitochondria could also be analysed by TEM as changes in mitochondria cristae and its membrane density are some of the ferroptosis main characteristics [128]. To add to the images, mitochondria markers could also be investigated to aggregate information between mitophagy and ferroptosis, such as mitoferritin 1 and 2. These mitoferritin are responsible for transporting iron into and out of the mitochondria membrane, and they are impaired in neurological diseases, which are related to ferroptosis [128]. Therefore, further analysis of iron transport in mitochondria would add great insight of how the cell respond to the iron overload environment needed in the ferroptosis-induced cell death.

Another possible approach is to test the conditions from my study by liquid chromatography with mass spectrometry (LC-MS/MS) analysis. Other researches have shown that unbiased lipidomics analyses can provide detailed information on lipid oxidation products and possible pathways which could help in indicating potent candidates for ferroptosis biomarkers [75]. Therefore, testing the conditions from my study by lipidomics could give important guidelines for future studies.

Ferroptosis is still a fairly new discovery in the field, and there is much more that can be explored to confirm the insights made in my research as discussed in detail above, particularly in skeletal muscle cells. By generating new knowledge of ferroptosis mechanism and adding new possibilities for finding new pharmacological compounds, such as ALY688, new approaches can be developed to help regulate cardiovascular diseases, diabetes, liver diseases and cancer.

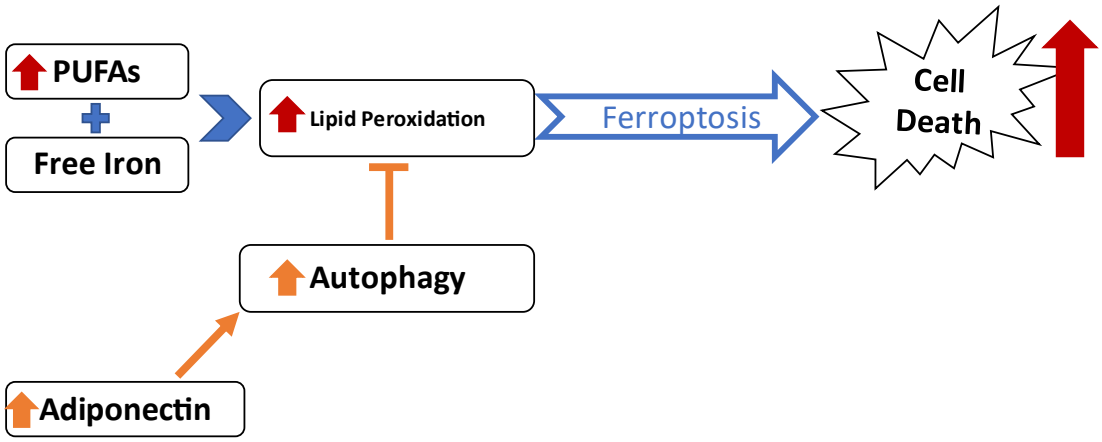

Figure 5.1: Impact of PUFAs and iron leading to ferroptotic-induced cell death, plus the protective role of autophagy in this process.

Possible effect of excess PUFAs changes cell susceptibility in the presence of low concentration of iron leading to an increase of lipid peroxidation, consequently, ferroptosis-induced cell death. In addition, the increase of adiponectin, an autophagy inducer, showed a possible protective effect against this iron-induced ferroptosis cell death.

References

1. Jeejeebhoy, K., et al., *Family physician-led, team-based, lifestyle intervention in patients with metabolic syndrome: results of a multicentre feasibility project.* CMAJ Open, 2017. **5**(1): p. E229-E236.
2. Canada, P.H.A.o. *Canadian Risk Factor Atlas (CRFA)*. 2020 edition.
3. Grundy, S.M., *Obesity, metabolic syndrome, and cardiovascular disease.* The Journal of Clinical Endocrinology & Metabolism, 2004. **89**(6): p. 2595-2600.
4. Hall, J.E., et al., *Obesity, kidney dysfunction and hypertension: mechanistic links.* Nat Rev Nephrol, 2019. **15**(6): p. 367-385.
5. Lavallard, V.J., et al., *Autophagy, signaling and obesity.* Pharmacological Research, 2012. **66**(6): p. 513-525.
6. Bray, G.A., et al., *The Science of Obesity Management: An Endocrine Society Scientific Statement.* Endocr Rev, 2018. **39**(2): p. 79-132.
7. Choe, S.S., et al., *Adipose Tissue Remodeling: Its Role in Energy Metabolism and Metabolic Disorders.* Frontiers in Endocrinology, 2016. **7**.
8. Richard, A.J., et al., *Adipose Tissue: Physiology to Metabolic Dysfunction*, in *Endotext*, K.R. Feingold, et al., Editors. 2000, MDText.com, Inc.

9. O'Rourke, R.W., *Adipose tissue and the physiologic underpinnings of metabolic disease.* Surg Obes Relat Dis, 2018. **14**(11): p. 1755-1763.
10. Hummasti, S. and G.S. Hotamisligil, *Endoplasmic Reticulum Stress and Inflammation in Obesity and Diabetes.* Circulation Research, 2010. **107**(5): p. 579-591.
11. Goodpaster, B.H. and D. Wolf, *Skeletal muscle lipid accumulation in obesity, insulin resistance, and type 2 diabetes.* Pediatric Diabetes, 2004. **5**(4): p. 219-226.
12. Longo, M., et al., *Adipose Tissue Dysfunction as Determinant of Obesity-Associated Metabolic Complications.* Int J Mol Sci, 2019. **20**(9).
13. Morales, P.E., J.L. Bucarey, and A. Espinosa, *Muscle Lipid Metabolism: Role of Lipid Droplets and Perilipins.* J Diabetes Res, 2017. **2017**: p. 1789395.

14. Tamilarasan, K.P., et al., *Skeletal muscle damage and impaired regeneration due to LPL-mediated lipotoxicity.* Cell Death & Disease, 2012. **3**(7): p. e354-e354.
15. Akhmedov, D. and R. Berdeaux, *The effects of obesity on skeletal muscle regeneration.* Frontiers in Physiology, 2013. **4**.
16. Wang, J. and K. Pantopoulos, *Regulation of cellular iron metabolism.* Biochem J, 2011. **434**(3): p. 365-81.
17. Chifman, J., R. Laubenbacher, and S.V. Torti, *A systems biology approach to iron metabolism.* Advances in experimental medicine and biology, 2014. **844**: p. 201-225.
18. Wang, Y., et al., *Iron Metabolism in Cancer.* International journal of molecular sciences, 2018. **20**(1): p. 95.
19. McDowell, L.A., P. Kudaravalli, and K.L. Sticco, *Iron Overload*, in *StatPearls*. 2022, StatPearls Publishing

20. Hamaï, A. and M. Mehrpour, *Homéostasie du fer et autophagie.* Med Sci (Paris), 2017. **33**(3): p. 260-267.
21. Jahng, J.W.S., et al., *Iron overload inhibits late stage autophagic flux leading to insulin resistance.* EMBO reports, 2019. **20**(10): p. e47911.
22. Sebastián, D. and A. Zorzano, *Self-Eating for Muscle Fitness: Autophagy in the Control of Energy Metabolism.* Dev Cell, 2020. **54**(2): p. 268-281.
23. Ahlstrom, P., et al., *Adiponectin improves insulin sensitivity via activation of autophagic flux.* Journal of Molecular Endocrinology, 2017. **59**(4): p. 339-350.
24. Frontera, W.R. and J. Ochala, *Skeletal muscle: a brief review of structure and function.* Calcif Tissue Int, 2015. **96**(3): p. 183-95.
25. Ikeda, Y., et al., *Iron-induced skeletal muscle atrophy involves an Akt-forkhead box O3-E3 ubiquitin ligase-dependent pathway.* J Trace Elem Med Biol, 2016. **35**: p. 66-76.
26. Wallace, D.F., *The Regulation of Iron Absorption and Homeostasis.* Clin Biochem Rev, 2016. **37**(2): p. 51-62.
27. Liu, J., R. Kang, and D. Tang, *Signaling pathways and defense mechanisms of ferroptosis.* Febs j, 2021.
28. Galluzzi, L., et al., *Cell death modalities: classification and pathophysiological implications.* Cell Death Differ, 2007. **14**(7): p. 1237-43.

29. Green, D.R. and F. Llambi, *Cell Death Signaling.* Cold Spring Harbor perspectives in biology, 2015. **7**(12): p. a006080.

30. Chen, Y., et al., *Distinct Types of Cell Death and the Implication in Diabetic Cardiomyopathy.* Frontiers in Pharmacology, 2020. **11**.

31. Dupont-Versteegden, E.E., *Apoptosis in skeletal muscle and its relevance to atrophy.* World journal of gastroenterology, 2006. **12**(46): p. 7463-7466.

32. Elmore, S., *Apoptosis: a review of programmed cell death.* Toxicol Pathol, 2007. **35**(4): p. 495-516.

33. Li, J., et al., *Ferroptosis: past, present and future.* Cell Death & Disease, 2020. **11**(2): p. 88.

34. Galluzzi, L., et al., *Molecular mechanisms of cell death: recommendations of the Nomenclature Committee on Cell Death 2018.* Cell Death & Differentiation, 2018. **25**(3): p. 486-541.

35. Dixon, S.J., et al., *Ferroptosis: an iron-dependent form of nonapoptotic cell death.* Cell, 2012. **149**(5): p. 1060-72.

36. Ju, J., Y.-N. Song, and K. Wang, *Mechanism of Ferroptosis: A Potential Target for Cardiovascular Diseases Treatment.* Aging and disease, 2021. **12**(1): p. 261-276.

37. Barrera, G., *Oxidative stress and lipid peroxidation products in cancer progression and therapy.* ISRN Oncol, 2012. **2012**: p. 137289.

38. Ayala, A., M.F. Muñoz, and S. Argüelles, *Lipid peroxidation: production, metabolism, and signaling mechanisms of malondialdehyde and 4-hydroxy-2-nonenal.* Oxidative medicine and cellular longevity, 2014. **2014**: p. 360438-360438.

39. Yang, W.S. and B.R. Stockwell, *Ferroptosis: Death by Lipid Peroxidation.* Trends Cell Biol, 2016. **26**(3): p. 165-176.

40. Lu, B., et al., *The Role of Ferroptosis in Cancer Development and Treatment Response.* Frontiers in Pharmacology, 2018. **8**.

41. Du, H., et al., *Research Progress of Ferroptosis in Adiposity-Based Chronic Disease (ABCD).* Oxid Med Cell Longev, 2022. **2022**: p. 1052699.

42. Ran, Q., et al., *Glutathione peroxidase 4 protects cortical neurons from oxidative injury and amyloid toxicity.* J Neurosci Res, 2006. **84**(1): p. 202-8.

43. Yagoda, N., et al., *RAS–RAF–MEK-dependent oxidative cell death involving voltage-dependent anion channels.* Nature, 2007. **447**(7146): p. 865-869.

44. Xie, Y., et al., *Ferroptosis: process and function.* Cell Death & Differentiation, 2016. **23**(3): p. 369-379.

45. Tang, D. and G. Kroemer, *Ferroptosis.* Current Biology, 2020. **30**(21): p. R1292-R1297.

46. Skouta, R., et al., *Ferrostatins inhibit oxidative lipid damage and cell death in diverse disease models.* J Am Chem Soc, 2014. **136**(12): p. 4551-6.

47. Yan, H.-f., et al., *Ferroptosis: mechanisms and links with diseases.* Signal Transduction and Targeted Therapy, 2021. **6**(1): p. 49.

48. Lei, P., T. Bai, and Y. Sun, *Mechanisms of Ferroptosis and Relations With Regulated Cell Death: A Review.* Frontiers in Physiology, 2019. **10**.

49. Wang, J., et al., *The Cross-Link between Ferroptosis and Kidney Diseases.* Oxidative Medicine and Cellular Longevity, 2021. **2021**: p. 6654887.

50. Jiang, X., B.R. Stockwell, and M. Conrad, *Ferroptosis: mechanisms, biology and role in disease.* Nature reviews. Molecular cell biology, 2021. **22**(4): p. 266-282.

51. Chen, X., R. Kang, and D. Tang, *Ferroptosis by Lipid Peroxidation: The Tip of the Iceberg?* Frontiers in Cell and Developmental Biology, 2021. **9**.

52. Kang, R. and D. Tang, *Autophagy and Ferroptosis—What Is the Connection?* Current Pathobiology Reports, 2017. **5**(2): p. 153-159.

53. Dixon, S.J., et al., *Human Haploid Cell Genetics Reveals Roles for Lipid Metabolism Genes in Nonapoptotic Cell Death.* ACS Chemical Biology, 2015. **10**(7): p. 1604-1609.

54. Feng, H., et al., *Transferrin Receptor Is a Specific Ferroptosis Marker.* Cell Rep, 2020. **30**(10): p. 3411-3423.e7.

55. Seibt, T.M., B. Proneth, and M. Conrad, *Role of GPX4 in ferroptosis and its pharmacological implication.* Free Radical Biology and Medicine, 2019. **133**: p. 144-152.

56. Stockwell, B.R., et al., *Ferroptosis: A Regulated Cell Death Nexus Linking Metabolism, Redox Biology, and Disease.* Cell, 2017. **171**(2): p. 273-285.

57. Qin, X., et al., *Ferritinophagy is involved in the zinc oxide nanoparticles-induced ferroptosis of vascular endothelial cells.* Autophagy, 2021. **17**(12): p. 4266-4285.

58. Stockwell, B.R., X. Jiang, and W. Gu, *Emerging Mechanisms and Disease Relevance of Ferroptosis.* Trends Cell Biol, 2020. **30**(6): p. 478-490.

59. Brown, C.W., et al., *Prominin2 Drives Ferroptosis Resistance by Stimulating Iron Export.* Dev Cell, 2019. **51**(5): p. 575-586.e4.

60. Doll, S. and M. Conrad, *Iron and ferroptosis: A still ill-defined liaison.* IUBMB Life, 2017. **69**(6): p. 423-434.

61. Friedmann Angeli, J.P., et al., *Inactivation of the ferroptosis regulator Gpx4 triggers acute renal failure in mice.* Nature cell biology, 2014. **16**(12): p. 1180-1191.

62. Zhang, C., et al., *Ferroptosis in cancer therapy: a novel approach to reversing drug resistance.* Molecular Cancer, 2022. **21**(1): p. 47.

63. Chen, X., et al., *Ferroptosis: machinery and regulation.* Autophagy, 2021. **17**(9): p. 2054-2081.

64. Kapoor, B., et al., *Dietary Polyunsaturated Fatty Acids (PUFAs): Uses and Potential Health Benefits.* Current Nutrition Reports, 2021. **10**(3): p. 232-242.

65. Sokoła-Wysoczańska, E., et al., *Polyunsaturated Fatty Acids and Their Potential Therapeutic Role in Cardiovascular System Disorders-A Review.* Nutrients, 2018. **10**(10).

66. Tallima, H. and R. El Ridi, *Arachidonic acid: Physiological roles and potential health benefits - A review.* J Adv Res, 2018. **11**: p. 33-41.

67. Hanna, V.S. and E.A.A. Hafez, *Synopsis of arachidonic acid metabolism: A review.* J Adv Res, 2018. **11**: p. 23-32.

68. Goodman, J.E., et al., *Arachidonate lipoxygenase (ALOX) and cyclooxygenase (COX) polymorphisms and colon cancer risk.* Carcinogenesis, 2004. **25**(12): p. 2467-2472.

69. Mashima, R. and T. Okuyama, *The role of lipoxygenases in pathophysiology; new insights and future perspectives.* Redox Biol, 2015. **6**: p. 297-310.

70. Hassannia, B., P. Vandenabeele, and T. Vanden Berghe, *Targeting Ferroptosis to Iron Out Cancer.* Cancer Cell, 2019. **35**(6): p. 830-849.

71. Chen, X., et al., *Organelle-specific regulation of ferroptosis.* Cell Death & Differentiation, 2021. **28**(10): p. 2843-2856.

72. Yu, Y., et al., *Ferroptosis: a cell death connecting oxidative stress, inflammation and cardiovascular diseases.* Cell Death Discovery, 2021. **7**(1): p. 193.

73. Wiernicki, B., et al., *Excessive phospholipid peroxidation distinguishes ferroptosis from other cell death modes including pyroptosis.* Cell Death & Disease, 2020. **11**(10): p. 922.
74. Agmon, E., et al., *Modeling the effects of lipid peroxidation during ferroptosis on membrane properties.* Scientific Reports, 2018. **8**(1): p. 5155.
75. Bayır, H., et al., *Achieving Life through Death: Redox Biology of Lipid Peroxidation in Ferroptosis.* Cell Chemical Biology, 2020. **27**(4): p. 387-408.
76. Sharma, A. and S.J.S. Flora, *Positive and Negative Regulation of Ferroptosis and Its Role in Maintaining Metabolic and Redox Homeostasis.* Oxid Med Cell Longev, 2021. **2021**: p. 9074206.
77. Yan, Y., G. Lei, and B. Gan, *A mTORC1-mediated cyst(e)ine sensing mechanism governing GPX4 synthesis and ferroptosis.* Mol Cell Oncol, 2021. **8**(3): p. 1919006.
78. Hou, W., et al., *Autophagy promotes ferroptosis by degradation of ferritin.* Autophagy, 2016. **12**(8): p. 1425-8.
79. Gao, M., et al., *Ferroptosis is an autophagic cell death process.* Cell Research, 2016. **26**(9): p. 1021-1032.
80. Dixon, S.J. and B.R. Stockwell, *The Hallmarks of Ferroptosis.* Annual Review of Cancer Biology, 2019. **3**(1): p. 35-54.
81. Zhou, Y., et al., *The crosstalk between autophagy and ferroptosis: what can we learn to target drug resistance in cancer?* Cancer Biol Med, 2019. **16**(4): p. 630-646.
82. Park, E. and S.W. Chung, *ROS-mediated autophagy increases intracellular iron levels and ferroptosis by ferritin and transferrin receptor regulation.* Cell Death & Disease, 2019. **10**(11): p. 822.
83. Runwal, G., et al., *LC3-positive structures are prominent in autophagy-deficient cells.* Scientific Reports, 2019. **9**(1): p. 10147.
84. Xiong, Q., et al., *WDR45 Mutation Impairs the Autophagic Degradation of Transferrin Receptor and Promotes Ferroptosis.* Frontiers in Molecular Biosciences, 2021. **8**.
85. Liu, J., et al., *Autophagy-Dependent Ferroptosis: Machinery and Regulation.* Cell Chemical Biology, 2020. **27**(4): p. 420-435.

86. Lin, M.G. and J.H. Hurley, *Structure and function of the ULK1 complex in autophagy.* Curr Opin Cell Biol, 2016. **39**: p. 61-8.

87. Kundu, M., *ULK1, mammalian target of rapamycin, and mitochondria: linking nutrient availability and autophagy.* Antioxid Redox Signal, 2011. **14**(10): p. 1953-8.

88. Funderburk, S.F., Q.J. Wang, and Z. Yue, *The Beclin 1-VPS34 complex--at the crossroads of autophagy and beyond.* Trends Cell Biol, 2010. **20**(6): p. 355-62.

89. Xu, F., et al., *Modulation of Autophagy: A Novel "Rejuvenation" Strategy for the Aging Liver.* Oxidative Medicine and Cellular Longevity, 2021. **2021**: p. 6611126.

90. Mariño, G., et al., *Self-consumption: the interplay of autophagy and apoptosis.* Nat Rev Mol Cell Biol, 2014. **15**(2): p. 81-94.

91. Mizushima, N., *Autophagy: process and function.* Genes Dev, 2007. **21**(22): p. 2861-73.

92. Kuma, A., et al., *The role of autophagy during the early neonatal starvation period.* Nature, 2004. **432**(7020): p. 1032-6.

93. Sandri, M., *Autophagy in skeletal muscle.* FEBS Lett, 2010. **584**(7): p. 1411-6.

94. Bjørkøy, G., et al., *Monitoring autophagic degradation of p62/SQSTM1.* Methods Enzymol, 2009. **452**: p. 181-97.

95. He, C. and D.J. Klionsky, *Regulation mechanisms and signaling pathways of autophagy.* Annu Rev Genet, 2009. **43**: p. 67-93.

96. Codogno, P. and A.J. Meijer, *Autophagy and signaling: their role in cell survival and cell death.* Cell Death & Differentiation, 2005. **12**(2): p. 1509-1518.

97. Li, J., et al., *Tumor heterogeneity in autophagy-dependent ferroptosis.* Autophagy, 2021. **17**(11): p. 3361-3374.

98. Chang, N.C., *Autophagy and Stem Cells: Self-Eating for Self-Renewal.* Frontiers in Cell and Developmental Biology, 2020. **8**.

99. Yamauchi, T., et al., *Adiponectin stimulates glucose utilization and fatty-acid oxidation by activating AMP-activated protein kinase.* Nature Medicine, 2002. **8**(11): p. 1288-1295.

100. Achari, A.E. and S.K. Jain, *Adiponectin, a Therapeutic Target for Obesity, Diabetes, and Endothelial Dysfunction.* Int J Mol Sci, 2017. **18**(6).

101. Fang, X. and G. Sweeney, *Mechanisms regulating energy metabolism by adiponectin in obesity and diabetes.* Biochem Soc Trans, 2006. **34**(Pt 5): p. 798-801.

102. Park, S.E., C.Y. Park, and G. Sweeney, *Biomarkers of insulin sensitivity and insulin resistance: Past, present and future.* Crit Rev Clin Lab Sci, 2015. **52**(4): p. 180-90.

103. M[ac]Donald, I.J., et al., *Associations between Adipokines in Arthritic Disease and Implications for Obesity.* Int J Mol Sci, 2019. **20**(6).

104. Yamauchi, T., et al., *Cloning of adiponectin receptors that mediate antidiabetic metabolic effects.* Nature, 2003. **423**(6941): p. 762-9.

105. Da Eira, D., et al., *Effects of the adiponectin mimetic compound ALY688 on glucose and fat metabolism in visceral and subcutaneous rat adipocytes.* Adipocyte, 2020. **9**(1): p. 550-562.

106. Liu, Y. and G. Sweeney, *Adiponectin action in skeletal muscle.* Best Practice & Research Clinical Endocrinology & Metabolism, 2014. **28**(1): p. 33-41.

107. Liu, Y., et al., *Adiponectin stimulates autophagy and reduces oxidative stress to enhance insulin sensitivity during high-fat diet feeding in mice.* Diabetes, 2015. **64**(1): p. 36-48.

108. Sung, H.K., et al., *ALY688 elicits adiponectin-mimetic signaling and improves insulin action in skeletal muscle cells.* American Journal of Physiology-Cell Physiology, 2022. **322**(2): p. C151-C163.

109. Gustafsson, Å.B. and R.A. Gottlieb, *Autophagy in Ischemic Heart Disease.* Circulation Research, 2009. **104**(2): p. 150-158.

110. Egnatchik, R.A., et al., *Palmitate-induced activation of mitochondrial metabolism promotes oxidative stress and apoptosis in H4IIEC3 rat hepatocytes.* Metabolism: clinical and experimental, 2014. **63**(2): p. 283-295.

111. Feng, H. and B.R. Stockwell, *Unsolved mysteries: How does lipid peroxidation cause ferroptosis?* PLoS Biol, 2018. **16**(5): p. e2006203.

112. Cheng, J.Z., et al., *Accelerated metabolism and exclusion of 4-hydroxynonenal through induction of RLIP76 and hGST5.8 is an early adaptive response of cells to heat and oxidative stress.* J Biol Chem, 2001. **276**(44): p. 41213-23.

113. Ruef, J., et al., *Induction of rat aortic smooth muscle cell growth by the lipid peroxidation product 4-hydroxy-2-nonenal.* Circulation, 1998. **97**(11): p. 1071-8.

114. García-Ruiz, I., et al., *Sp1 and Sp3 transcription factors mediate malondialdehyde-induced collagen alpha 1(I) gene expression in cultured hepatic stellate cells.* J Biol Chem, 2002. **277**(34): p. 30551-8.

115. Hao, S., et al., *Metabolic networks in ferroptosis.* Oncol Lett, 2018. **15**(4): p. 5405-5411.

116. Sousa, L., et al., *Iron overload: Effects on cellular biochemistry.* Clinica Chimica Acta, 2020. **504**: p. 180-189.

117. Tang, D., et al., *Ferroptosis: molecular mechanisms and health implications.* Cell Research, 2021. **31**(2): p. 107-125.

118. Persson, H.L., K.J. Nilsson, and U.T. Brunk, *Novel cellular defenses against iron and oxidation: ferritin and autophagocytosis preserve lysosomal stability in airway epithelium.* Redox Report, 2001. **6**(1): p. 57-63.

119. Dhayal, S., et al., *Differential effects of saturated and unsaturated fatty acids on autophagy in pancreatic β-cells.* Journal of Molecular Endocrinology, 2019. **63**(4): p. 285-296.

120. Liu, J., et al., *Crosstalk Between Autophagy and Ferroptosis and Its Putative Role in Ischemic Stroke.* Frontiers in Cellular Neuroscience, 2020. **14**.

121. Nguyen, T.M.D., *Adiponectin: Role in Physiology and Pathophysiology.* Int J Prev Med, 2020. **11**: p. 136.

122. Yuan, H., et al., *Identification of ACSL4 as a biomarker and contributor of ferroptosis.* Biochem Biophys Res Commun, 2016. **478**(3): p. 1338-43.

123. Latunde-Dada, G.O., *Ferroptosis: Role of lipid peroxidation, iron and ferritinophagy.* Biochim Biophys Acta Gen Subj, 2017. **1861**(8): p. 1893-1900.

124. Fang, Y., et al., *Inhibiting Ferroptosis through Disrupting the NCOA4-FTH1 Interaction: A New Mechanism of Action.* ACS Cent Sci, 2021. **7**(6): p. 980-989.

125. Zhou, C., et al., *Monitoring autophagic flux by an improved tandem fluorescent-tagged LC3 (mTagRFP-mWasabi-LC3) reveals that high-dose rapamycin impairs autophagic flux in cancer cells.* Autophagy, 2012. **8**(8): p. 1215-26.

126. Zhou, T., et al., *Mild hypothermia protects hippocampal neurons against oxygen-glucose deprivation/reperfusion-induced injury by improving lysosomal function and autophagic flux.* Experimental Cell Research, 2017. **358**(2): p. 147-160.

127. Renna, M., et al., *Chemical inducers of autophagy that enhance the clearance of mutant proteins in neurodegenerative diseases.* J Biol Chem, 2010. **285**(15): p. 11061-7.
128. Battaglia, A.M., et al., *Ferroptosis and Cancer: Mitochondria Meet the "Iron Maiden" Cell Death.* Cells, 2020. **9**(6).

Appendix A: List of Contributions

This thesis was written and researched by Patricia de Menezes Reboucas (PR). PR worked with Abdul Hadee Lone (AL) to complete the flow cytometry data (Figure 3.6). PR grew the cells, treated, stained, washed and harvested. AL performed the rest of the experiment in the flow cytometry. AL also helped with the statistical analysis and graphing, particularly Fig 3.6**B**.

Appendix B: Permission for use of adapted or reproduced figures from websites or articles

Figure 1.1: Retrieved from Ju, J. 2020 [36]. Open Access article.

Ju, J., Y.-N. Song, and K. Wang, *Mechanism of Ferroptosis: A Potential Target for Cardiovascular Diseases Treatment.* Aging and disease, 2021. **12**(1): p. 261-276.

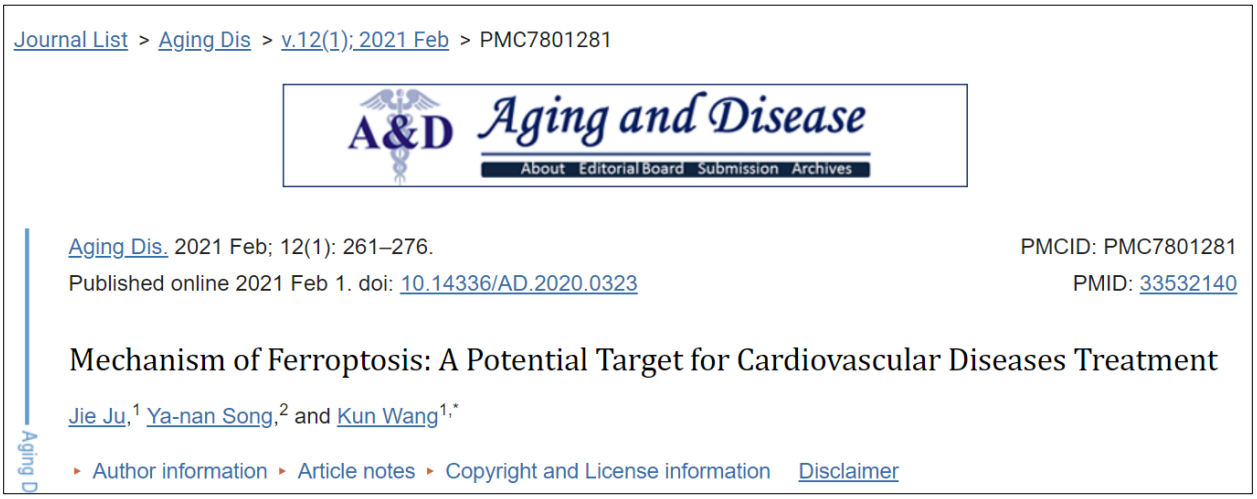

Journal List > Aging Dis > v.12(1); 2021 Feb > PMC7801281

A&D Aging and Disease

About Editorial Board Submission Archives

Aging Dis. 2021 Feb; 12(1): 261–276. PMCID: PMC7801281

Published online 2021 Feb 1. doi: 10.14336/AD.2020.0323 PMID: 33532140

Mechanism of Ferroptosis: A Potential Target for Cardiovascular Diseases Treatment

Jie Ju,[1] Ya-nan Song,[2] and Kun Wang[1,*]

Author information Article notes Copyright and License information Disclaimer

Figure 1.2: Image retrieved and adapted from Lu, B., et al (2018) [40]. Open Access article.

Lu, B., et al., *The Role of Ferroptosis in Cancer Development and Treatment Response.* Frontiers in Pharmacology, 2018. **8**.

Figure 1.3: Image retrieved and adapted from Chang, N.C. (2020) [98]. Open Access article.

Chang, N.C., *Autophagy and Stem Cells: Self-Eating for Self-Renewal.* Frontiers in Cell and Developmental Biology, 2020. **8**.

Figure 3.9: Image retrieved from ThermoFisher website (https://assets.thermofisher.com/TFS-Assets/BID/brochures/cellinsight-cx5-cx7-led-cx7-lzr-high-content-screening-platforms-brochure.pdf).

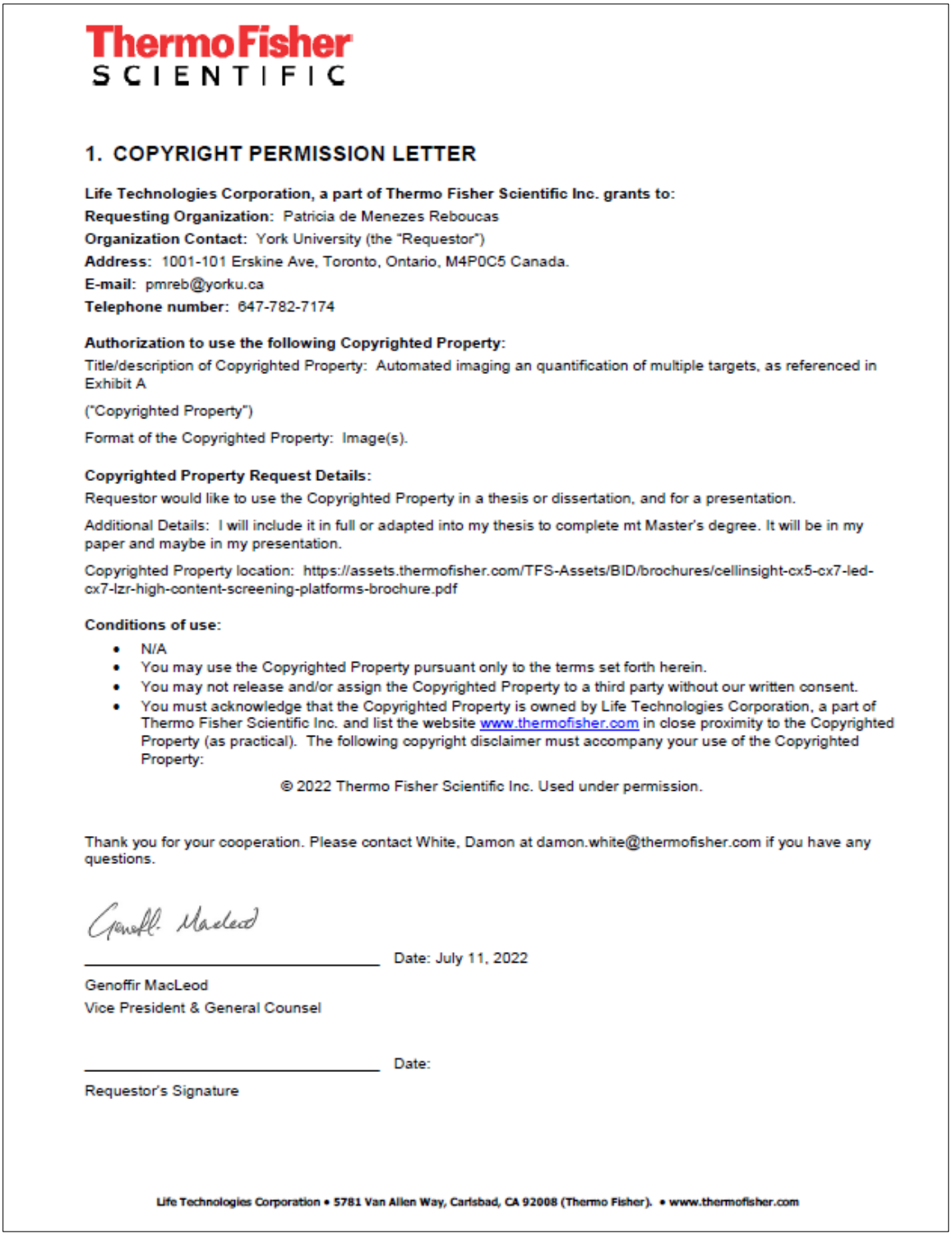

ThermoFisher SCIENTIFIC

1. COPYRIGHT PERMISSION LETTER

Life Technologies Corporation, a part of Thermo Fisher Scientific Inc. grants to:
Requesting Organization: Patricia de Menezes Reboucas
Organization Contact: York University (the "Requestor")
Address: 1001-101 Erskine Ave, Toronto, Ontario, M4P0C5 Canada.
E-mail: pmreb@yorku.ca
Telephone number: 647-782-7174

Authorization to use the following Copyrighted Property:
Title/description of Copyrighted Property: Automated imaging an quantification of multiple targets, as referenced in Exhibit A

("Copyrighted Property")

Format of the Copyrighted Property: Image(s).

Copyrighted Property Request Details:
Requestor would like to use the Copyrighted Property in a thesis or dissertation, and for a presentation.

Additional Details: I will include it in full or adapted into my thesis to complete mt Master's degree. It will be in my paper and maybe in my presentation.

Copyrighted Property location: https://assets.thermofisher.com/TFS-Assets/BID/brochures/cellinsight-cx5-cx7-led-cx7-lzr-high-content-screening-platforms-brochure.pdf

Conditions of use:

- N/A
- You may use the Copyrighted Property pursuant only to the terms set forth herein.
- You may not release and/or assign the Copyrighted Property to a third party without our written consent.
- You must acknowledge that the Copyrighted Property is owned by Life Technologies Corporation, a part of Thermo Fisher Scientific Inc. and list the website www.thermofisher.com in close proximity to the Copyrighted Property (as practical). The following copyright disclaimer must accompany your use of the Copyrighted Property:

  © 2022 Thermo Fisher Scientific Inc. Used under permission.

Thank you for your cooperation. Please contact White, Damon at damon.white@thermofisher.com if you have any questions.

Genoffir MacLeod

_____ Date: July 11, 2022

Genoffir MacLeod
Vice President & General Counsel

_____ Date:

Requestor's Signature

Life Technologies Corporation • 5781 Van Allen Way, Carlsbad, CA 92008 (Thermo Fisher). • www.thermofisher.com